

INFLUENCE OF CONFINED CONCRETE MODELS ON THE SEISMIC
RESPONSE OF RC FRAMES

A THESIS SUBMITTED TO
THE FACULTY OF ARCHITECTURE AND ENGINEERING
OF
EPOKA UNIVERSITY

BY

BREDLI PLAKU

IN PARTIAL FULFILLMENT OF THE REQUIREMENTS
FOR
THE DEGREE OF MASTER OF SCIENCE
IN
CIVIL ENGINEERING

JULY, 2023

Approval sheet of the Thesis

This is to certify that we have read this thesis entitled “**Influence of Confined Concrete Models on the Seismic Response of RC Frames**” and that in our opinion it is fully adequate, in scope and quality, as a thesis for the degree of Master of Science.

Assoc. Prof. Dr. Mirjam Ndini
Head of Department
Date: July, 04, 2023

Examining Committee Members:

Prof. Dr. Hüseyin Bilgin (Civil Engineering) _____

Assoc. Prof. Dr. Mirjam Ndini (Civil Engineering) _____

Dr. Marsed Leti (Civil Engineering) _____

I hereby declare that all information in this document has been obtained and presented in accordance with academic rules and ethical conduct. I also declare that, as required by these rules and conduct, I have fully cited and referenced all material and results that are not original to this work.

Name Surname: Bredli Plaku

Signature: _____

ABSTRACT

Influence of Confined Concrete Models on the Seismic Response of RC Frames

Plaku, Bredli

Master of Science, Department of Civil Engineering

Supervisor: Prof. Dr. Hüseyin Bilgin

In this thesis, the influence of confined concrete models on the response of reinforced concrete structures is investigated at member and global system levels. The commonly encountered concrete models such as Modified Kent-Park, Saatçioğlu-Razvi and Mander are considered. Two moment-resisting frames designed according to the pre-modern code are taken into consideration to reflect the example of a RC moment-resisting frame in the current building stock. The building is in an earthquake-prone zone to be located on Z3 Soil Type. The inelastic response of the building frame is modelled by considering the plastic hinges formed on each beam and column element for different concrete classes and stirrups spacings. The models are subjected to non-linear static analyses. The differences between confined concrete models are comparatively investigated at both reinforced concrete member and system levels. Based on the results of the analyses, it is observed that the differences exhibited in the moment-curvature response of column cross-sections do not significantly affect the overall behaviour of the global system.

Keywords: *Non-linear static analysis, moment-curvature relationships, plastic hinges, concrete confinement models, seismic action.*

ABSTRAKT

Influenca e Modeleve të Betonit të Kufizuar në Sjelljen Sizmike të Strukturave Betonarme

Plaku, Bredli

Master Shkencor, Departamenti i Inxhinierisë së Ndërtimit

Udhëheqësi: Prof. Dr. Hüseyin Bilgin

Në këtë tezë, ndikimi i modeleve të betonit të kufizuar në strukturat e betonit të armuar është studiuar në nivel elementi dhe global. Modelet e betonit që hasen më shpesh si Kent-Park i Modifikuar, Saatçioğlu-Razvi dhe Mander janë marrë në konsideratë. Dy ndërtesa rezistente ndaj momentit, të projektuara sipas kodeve paramoderne, janë marrë në konsideratë për të pasqyruar shembullin e strukturave të betonit nga stoku aktual i ndërtesave. Ndërtesa është në zonë tërmetesh e vendosur në llojin e dheut Z3. Sjellja joelastike e strukturës së ndërtesës është modeluar duke marrë në konsideratë menteshat plastike e formuara në çdo element trau dhe kolone për klasa të ndryshme të betonit. Modelet i janë nënshtruar analizave statike jolineare. Dallimet e modeleve të betonit të kufizuar janë studiuar në mënyrë krahasuese në nivel elementi dhe global. Bazuar në rezultatet e analizave vërehet se diferencat e shfaqura në sjelljen jolineare të kolonës nuk ndikojnë ndjeshëm në sjelljen e përgjithshme të sistemit global.

Fjalët kyçe: *Analiza statike jolineare, marrëdhënia moment-përkulje, mentesha plastike, modelet e kufizimit të betonit, veprimet sizmike.*

ACKNOWLEDGEMENTS

I wish to express my sincere gratitude to my supervisor, Prof. Dr. Hüseyin Bilgin and Dr. Marsed Leti for their guidance and support throughout my research.

I also want to express my thanks to my family for their support and encouragement throughout my academic years. Their trust in me and my work has always been the source of my motivation.

To everyone who has contributed to this thesis, thank you!

TABLE OF CONTENTS

ABSTRACT.....	iv
ABSTRAKT.....	v
ACKNOWLEDGEMENTS	vi
LIST OF TABLES	x
LIST OF FIGURES	xi
CHAPTER 1	1
INTRODUCTION	1
1.1 General	1
1.2 Objective of thesis	2
1.3 Scope of work and methodology.....	2
1.4 Organization of the thesis.....	2
CHAPTER 2	4
LITERATURE REVIEW.....	4
2.1 Plain Concrete	4
2.2 Prestressed Concrete.....	4
2.3 Reinforcement Steel	6
2.3.1 Types of Steel	6
2.3.2 Rebar Sizes	7
2.4 Reinforced Concrete.....	8
2.4.1 Unconfined Concrete	8
2.4.2 Confined Concrete	9

2.5	Stress-Strain Relationship	10
2.5.1	Stress Block Parameters.....	11
2.5.2	Stress-Strain of Steel.....	12
2.5.3	Stress-Strain of Concrete	16
CHAPTER 3		18
METHODOLOGY		18
3.1	Global and Local Levels.....	18
3.2	Confined Concrete Models.....	20
3.2.1	Modified Kent-Park Model.....	21
3.2.2	Saatçiođlu-Razvi Model	25
3.2.3	Mander Model.....	28
3.3	Moment-Curvature Relationship.....	30
3.3.1	Calculating Moment-Curvature according to Kent-Park Model	34
3.3.2	The Presence of Compressive Reinforcement.....	39
3.3.3	Comparison with worked examples.....	42
3.3.4	The Presence of Transverse Reinforcement	43
3.4	Moment-Rotation Relationship	44
CHAPTER 4		48
CASE STUDY		48
4.1	Four-Storey Residential Building.....	48
4.2	Seven-Storey Residential Building	56
CHAPTER 5		60
RESULTS AND DISCUSSIONS		60

5.1	Results	60
CHAPTER 6		65
CONCLUSIONS.....		65
6.1	Conclusions	65
6.2	Recommendations for future research.....	66

LIST OF TABLES

Table 1. Rebar Size Charts [11].	7
Table 2. Peak stress and strain for some concrete models [1]	21
Table 3. $P \rightarrow V \rightarrow M \rightarrow \phi \rightarrow \theta \rightarrow \delta$ Relationship [9]	33
Table 4. Calculated Moment-Curvature values	42
Table 5. Empirical equations for calculating the length of plastic hinges [29]	45
Table 6. Data for the first case	48
Table 7. Data for the second case	56

LIST OF FIGURES

Figure 1. Unloaded Prestressed Beam [8].....	5
Figure 2. Loaded Prestressed Beam [8]	5
Figure 3. Typical reinforcement steel shape [9].....	6
Figure 4. Plain concrete beam under a longitudinal load [8]	8
Figure 5. Properly reinforced unconfined concrete beam [8]	8
Figure 6. Improperly reinforced unconfined concrete beam [8]	9
Figure 7. Confined reinforced concrete column [12].....	9
Figure 8. Strain of a horizontal body	10
Figure 9. Stress-Strain relationship for different types of materials	11
Figure 10. Stress Block of a rectangular reinforced concrete section [13]	12
Figure 11. Stress-Strain curve for #8 bar (25.4 mm diameter) [9].....	12
Figure 12. Necking forming in the steel bar [14].....	13
Figure 13. Stress-Strain curve for several types of reinforcing steel [9]	13
Figure 14. Stress-strain curve for steel bars with different diameters. The 6 mm and 9 mm curves represent cold-worked steel bars [15].....	14
Figure 15. Idealised Stress-Strain Curve for Reinforcing Steel [9]	16
Figure 16. Compression Test Machine [19].....	17
Figure 17. Stress-Strain curve for Unconfined Concrete [21]	17
Figure 18. Global and Local Levels Hierarchy [2]	18

Figure 19. Locating plastic hinges from moment-curvature [2], [9].....	19
Figure 20. Typical plastic mechanisms for moment-resisting frames	20
Figure 21. Stress-Strain Relationship for Concrete proposed by Kent and Park [22]	22
Figure 22. Stress Block for the Modified Kent-Park Model [22]	22
Figure 23. Kent-Park model response under load cycles.....	24
Figure 24. Stress-Strain Relationship of Confined Concrete proposed by Saatçioğlu and Razvi [4].....	25
Figure 25. Stress-Strain Relationship of Concrete proposed by Mander [25]	28
Figure 26. Mander model response under load cycles [26]	30
Figure 27. Beam Member with a specific length and section [9]	30
Figure 28. Deflection curve of a beam under an axial load [9].....	31
Figure 29. Small section taken from a simply supported beam [9]	31
Figure 30. Moment-Curvature curve of an unconfined concrete beam [9].....	34
Figure 31. Transformation of the reinforced concrete cross-section to an equivalent concrete section [9]	35
Figure 32. The stress block at the cracking point [9].....	36
Figure 33. The stress block at the yielding point [9].....	37
Figure 34. The stress block at the ultimate load point [9].....	38
Figure 35. Stress Block at yielding point of doubly reinforced beam [9].....	40
Figure 36. Example of an unconfined concrete section	42
Figure 37. Graphic representation of the moment-curvature data	43

Figure 38. Confined Beam Section [9]	44
Figure 39. Typical location of plastic hinges [9]	44
Figure 40. Length of shear spans formed in a frame [30].....	47
Figure 41. Member cross-sections for the four-storey frame [6].....	49
Figure 42. Top view of the frame in xy plan [31].....	49
Figure 43. Side views of the frame in xz and yz plans respectively	50
Figure 44. Configuring the section in SEMAp [6].....	50
Figure 45. Generated stress-strain curves for the C250x500 column in Case 1.1	51
Figure 46. Generated moment-curvature curves for the C250x500 column in Case 1.1	52
Figure 47. Generated moment-rotation curve for the Modified Kent-Park model of the C250x500 column in Case 1.1	52
Figure 48. One of the most critical beams in the 4-storey frame.....	53
Figure 49. The most critical column in the middle of the frame.....	53
Figure 50. Defining the force-displacement parameters for shear, V2, of column....	54
Figure 51. Defining the moment-rotation parameters for moment, M2, of column ..	55
Figure 52. The parameters for the non-linear static pushover analysis in the y-direction	56
Figure 53. Member cross-sections for the seven-storey frame [6].....	57
Figure 54. Side view of the frame in xz and yz plans respectively.....	57
Figure 55. One of the most critical beams in the 4-storey frame.....	58
Figure 56. The most critical column in the middle of the frame.....	58

Figure 57. The parameters for the non-linear static pushover analysis in the x-direction	59
Figure 59. Moment-curvature data for the selected beam sections.....	60
Figure 59. Moment-curvature data for the selected column sections	61
Figure 60. Capacity curves for the four-storey frame	62
Figure 62. Capacity curves for seven-storey frame	63

CHAPTER 1

INTRODUCTION

1.1 General

Concrete is the most used material in construction due to its strength, durability, and versatility. It possesses excellent compressive strength, but it also has limited resistance to tensile forces.

To better understand and predict the behaviour of concrete, researchers have developed various concrete models that attempt to capture the complex interactions between the concrete, reinforcement, and external confining pressures. They are mathematical representations of the behaviour of concrete under different loading conditions used to simulate the stress-strain relationship, the failure criteria, and the post-failure behaviour of concrete elements in structural analysis. Some proposed concrete models are by Assa et al, Cusson and Paultre, El-Dash & Ahmad, Fafitis and Shah, Hoshikuma et al, Kent and Park, Mander et al, Mansur et al, Richart et al, Roy and Sozen, Saatcioglu and Ravi, Scott et al, Sheikh and Uzumer, Yong et al, etc [1].

There has been a notable trend in recent decades, particularly in the assessment of seismic behaviour of existing structures, towards displacement-based analysis methods instead of force-based methods. These methods consider the non-linear behaviour of structures, enabling more realistic results to be obtained. The structural elements, and consequently the non-linear behaviour of the structure, are modelled using plastic hinges determined according to the element properties [2]. Therefore, determining the behaviour of plastic hinges is a crucial part of the analysis for estimating the structure's behaviour.

1.2 Objective of thesis

This thesis aims to investigate the effects of different concrete models proposed by various researchers on the behaviour of reinforced concrete at element level and different concrete grades and reinforcement at system level. Two frame structures, a four-story and a seven-story one, have been considered for the analysis. The non-linear behaviour is expressed using the non-linear static pushover analysis method, which is widely used in research. The concrete models proposed by Kent-Part (1971) [3], Saatçioğlu-Razvi (1992) [4], and Mander (1994) [5] are considered.

By achieving these objectives, this thesis aims to contribute to the advancement of structural engineering and provide valuable information for the design and construction of safer and more resilient reinforced concrete structures.

1.3 Scope of work and methodology

This thesis focuses on the non-linear static analysis of two reinforced concrete frame structures: a four-storey and a seven-storey frame. The moment-curvature relationship is used to analyse the non-linear behaviour of the members at the element level, and the pushover analysis is used to investigate the non-linear behaviour of the frames at the global level. The non-linear static analysis has been conducted using the following tools:

- SEMAp [6]
- CSi SAP2000 [7]

1.4 Organization of the thesis

This thesis is divided into five chapters. The organization is done as follows:

- Chapter 1 introduces the information needed to understand the topic and lists the objectives that need to be answered at the end of this thesis.

- Chapter 2 gives an insight into the topic by other researchers and introduces the sources which have supported collecting the data.
- Chapter 3 consists of the methodology used to conduct the research and all the additional information.
- Chapter 4 includes all the results collected from the previous chapter and the comparison/investigation/deduction of this data.
- Chapter 5 consists of the conclusions, limitations to the research process and recommendations for further research.

CHAPTER 2

LITERATURE REVIEW

2.1 Plain Concrete

Concrete is one of the most used materials in construction since ancient times. It is a composite material made of:

- Fine aggregate, which provides stability, fills the voids between larger aggregates and contributes to the overall strength and workability of the concrete mixture.
- Coarse aggregate, which consists of larger particles, adds strength, volume stability, and load-bearing capacity to the concrete mixture.
- Water, which acts as a reactant in the chemical process called hydration, where water chemically reacts with cement to form a solid matrix. Water also provides workability to the concrete mix, allowing it to be easily poured, compacted, and shaped during construction.
- Cement, which when mixed with water undergoes the hydration process, forming a paste that binds the aggregate particles together, creating a cohesive and solid structure.

Plain concrete is used in applications where the primary load is compressive or where tensile stresses are minimal, such as pavements, walls, and foundations. Its compressive strength, durability, and relatively low cost make it a practical and widely used material in these contexts.

2.2 Prestressed Concrete

Just as the name implies, prestressed concrete is concrete that has been compressed during its production. By incorporating prestressing in concrete, structures

can achieve higher load-carrying capacity, improved resistance to cracking, and enhanced durability. The distribution of forces within a prestressed member helps optimize its structural performance and ensures efficient utilization of materials [8].

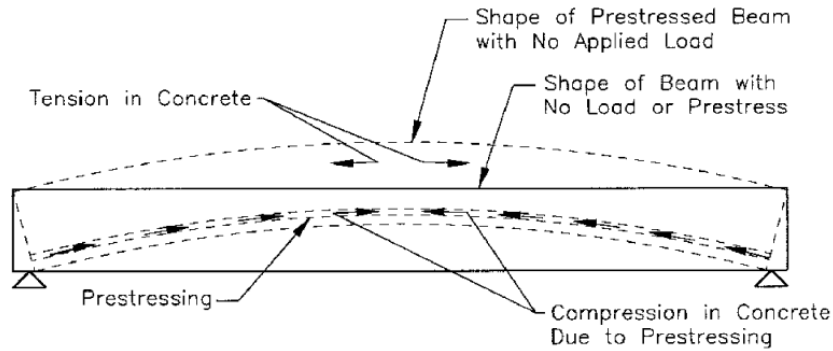


Figure 1. Unloaded Prestressed Beam [8]

Let's take a beam element as an example. The beam is initially "squeezed" or subjected to compressive forces to induce pre-compression. This pre-compression is achieved by tensioning high-strength steel tendons or cables within the concrete before it fully hardens. The tendons are anchored at the ends of the beam, and once the concrete has hardened, the tendons are released, transferring the compressive forces to the concrete (*Figure 1*).

This pre-compression allows the prestressed concrete beam to resist the tensile stresses that occur when the beam is loaded. The compressive forces counterbalance the external loads, resulting in reduced tensile stresses within the concrete. As a result, cracks and deformation that typically occur in non-prestressed concrete beams under load can be significantly minimized or eliminated.

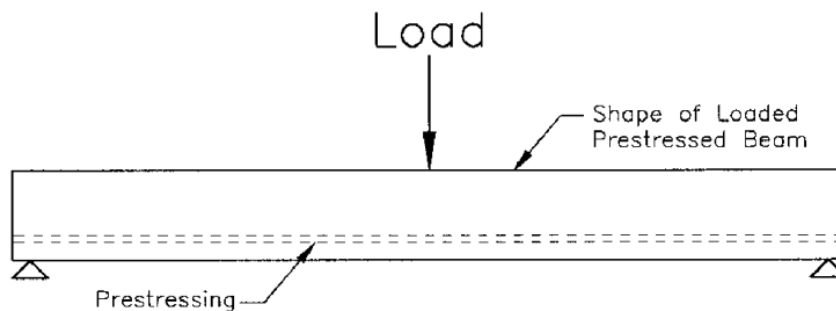


Figure 2. Loaded Prestressed Beam [8]

In the unloaded state, the pre-compression in the prestressed beam causes it to adopt a slightly curved shape, known as the default shape (*Figure 2*). The top section of the beam remains under compression, while the bottom section experiences reduced tension due to the pre-compression

2.3 Reinforcement Steel

The most common material used for reinforcing concrete is round deformed steel bars. The steel itself is straight, but the deformation is on its surface, as shown in *Figure 3*.

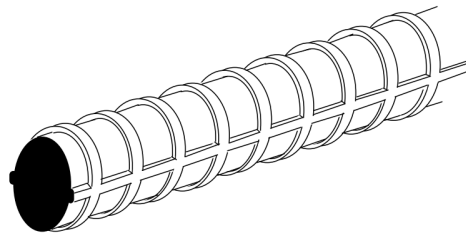


Figure 3. Typical reinforcement steel shape [9]

This rib-like shape creates a mechanical bond between the rough surface of concrete and the usually smooth surface of the steel.

2.3.1 Types of Steel

Steel reinforcement is classified into [10]:

- Mild Steel Bar, smooth and round. They are mostly used on roads and highways.
- Deformed Steel Bar, which have a rib-like surface. They are classified to:
 - Thermo-Mechanically Treated Bars (TMT).
 - High-Strength Deformed Bars.

- European Rebars, made of manganese and bend easily.
- Carbon Steel Rebar, made of carbon. The main disadvantage is that it corrodes easily.
- Epoxy-Coated Rebar, resistant to corrosion but very delicate coating.
- Galvanized Rebar, more resistant to corrosion but it costs more.
- Glass-Fibre-Reinforced-Polymer (GFRP).
- Stainless Steel Rebar, easy to bend and resistant to corrosion, but also the most expensive type of reinforcement.

Due to their workability and cost, High-Strength Deformed Bars are the most common reinforcement used in concrete.

2.3.2 Rebar Sizes

Deformed steel bars are classified by their cross-sectional diameter. The classification is done according to ASTM A 615M/A 615, A 706M/A 706, and A 996M/A 996 [8]. Depending on the country, the diameters are available in both S.I. Units and Imperial Units. The S.I. bar sizes are a derivative of the Imperial bar sizes.

Table 1. Rebar Size Charts [11].

U.S. Rebar Size Chart					European Rebar Size Chart		
Imperial Bar Size	Nominal Diameter		Nominal Area		Metric Bar Size	Nominal Diameter	Cross- Sectional Area
	(inch)	(mm)	(inch ²)	(mm ²)		(mm)	
#2	0.250	6.35	0.05	32	6	6	28.3
#3	0.375	9.525	0.11	71	8	8	50.3
#4	0.500	12.7	0.20	129	10	10	78.5
#5	0.625	15.875	0.31	200	12	12	113
#6	0.750	19.05	0.44	284	14	14	154
#7	0.875	22.225	0.60	387	16	16	201
#8	1.000	25.4	0.79	509	20	20	314
#9	1.128	28.65	1.00	645	25	25	491
#10	1.270	32.26	1.27	819	28	28	616
#11	1.410	35.81	1.56	1006	32	32	804
#14	1.693	43	2.25	1452	40	40	1257
#18	2.257	57.3	4.00	2581	50	50	1963

2.4 Reinforced Concrete

Reinforced concrete is a composite material that combines the compressive strength of concrete with the tensile strength of steel reinforcement. When a beam is subjected to vertical loads or a column is subjected to eccentric axial and lateral loads, it experiences flexural stresses that cause cracks to the region in tension and shear stresses that cause cracks near the supports (*Figure 4*).

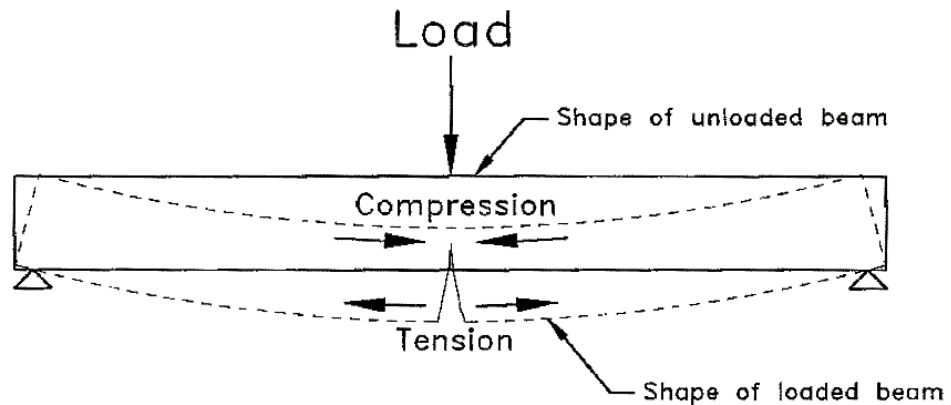


Figure 4. Plain concrete beam under a longitudinal load [8]

2.4.1 Unconfined Concrete

By incorporating longitudinal reinforcement at the regions with high tensile stress concentration, the capacity to withstand tensile forces is significantly enhanced, thus preventing the formation of cracks.

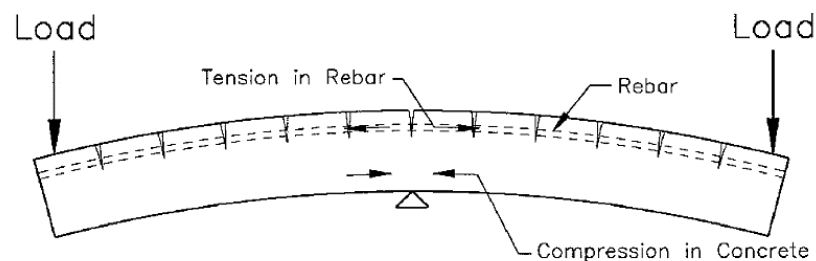


Figure 5. Properly reinforced unconfined concrete beam [8]

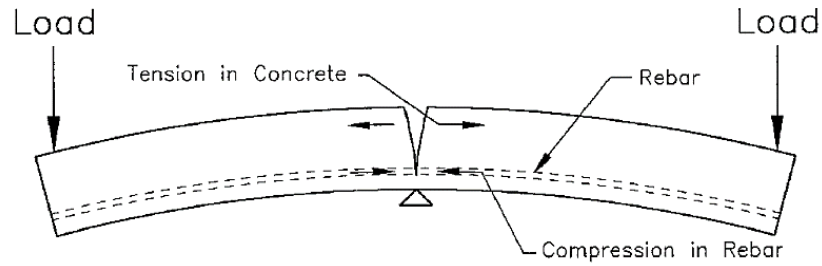


Figure 6. Improperly reinforced unconfined concrete beam [8]

Unconfined concrete is mostly used in foundations, pavements, and walls, where the shear stresses are minimal; and confined concrete is used in structural members that are subject to bending and shear stresses.

2.4.2 Confined Concrete

Similarly, by confining the longitudinal reinforcement using transverse reinforcement, the resistance to shear forces is increased. In contrast to unconfined concrete, confined concrete exhibits a ductile failure due to the presence of lateral reinforcement.

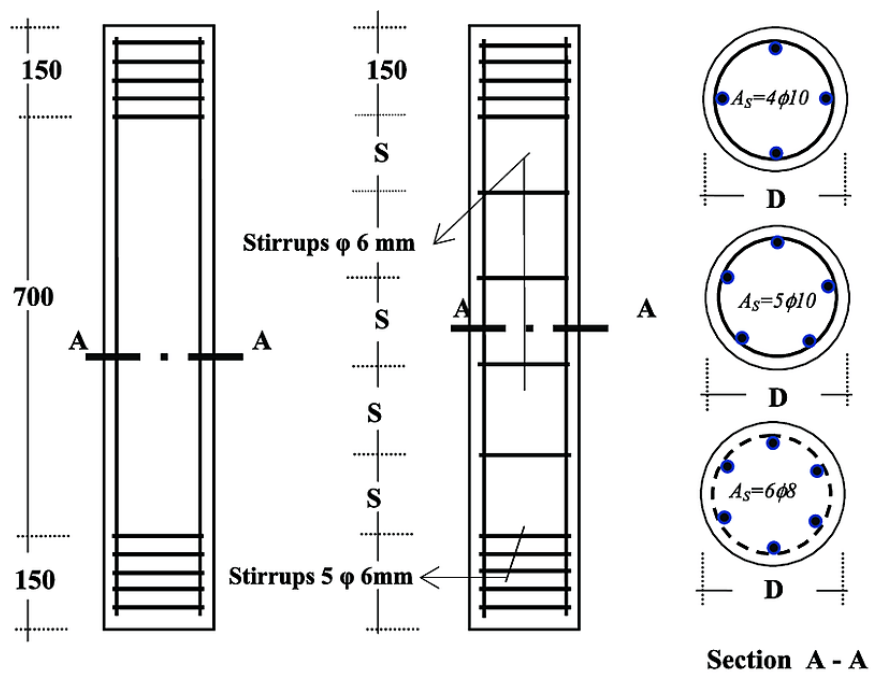


Figure 7. Confined reinforced concrete column [12]

2.5 Stress-Strain Relationship

The stress-strain relationship is the fundamental concept in the mechanics of a material. It describes the deformation of a material when a load is applied to it.

Strain is the ratio of change in the length of the body.

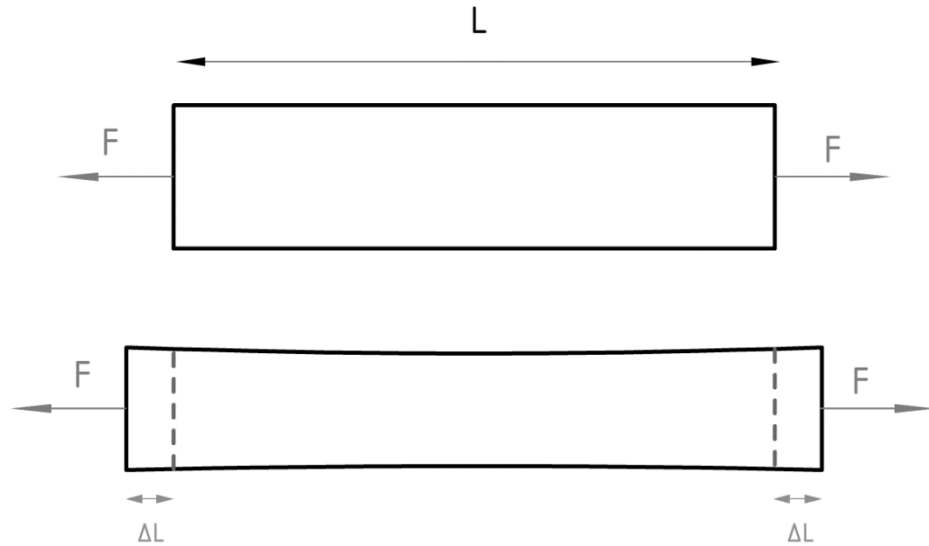


Figure 8. Strain of a horizontal body

$$\epsilon_x = \frac{\Delta L}{L} \quad (\text{Equation 1})$$

Stress is the internal resistance of the body under the effect of external forces.

$$\sigma = \frac{F}{A} \quad (\text{Equation 2})$$

where A is the area of the cross-section.

This relationship can be demonstrated in graphical form, where the curve describes the deformation when force is increased. The shape of the curve depends on the material's properties.

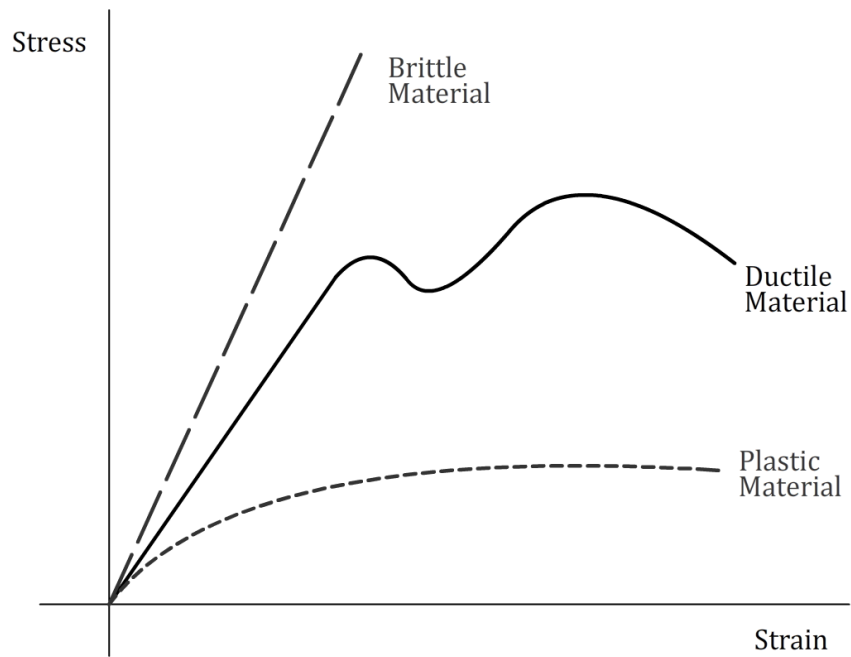


Figure 9. Stress-Strain relationship for different types of materials

- Brittle materials break with small elastic deformation. There is no plastic deformation.
 - Elastic limit = Yield strength = Ultimate tensile strength
- Ductile materials have both elastic and plastic deformations.
 - Elastic limit → Yield strength → Ultimate strength
- Plastic materials exhibit only plastic deformation.

Understanding the stress-strain relationship of concrete and steel is crucial for designing safe structures. The linear and non-linear behaviours that these materials exhibit must be considered to analyse their response under load [9].

2.5.1 Stress Block Parameters

The stress block model is a graphical representation of the stress distribution of a cross-section. In civil engineering, the tensile/compressive stresses are displayed for a member's (beam/column) cross-section. The stress block models used for reinforced concrete are:

- Triangular Stress Block, in which the stress distribution is nearly proportional to the strain. It is valid up to the Serviceability Limit State
- Parabolic Stress Block, in which the strains are within the plastic range. It is valid for the Ultimate Limit State.
 - Rectangular Stress Block is the simplified equivalent of the Parabolic Stress Block

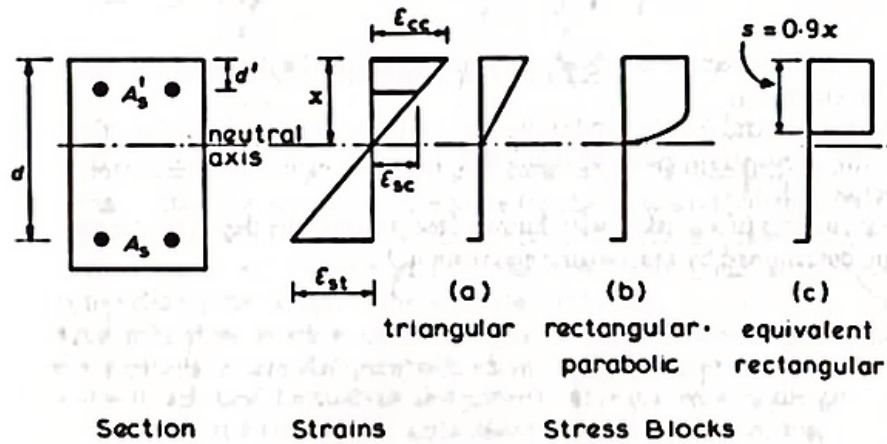


Figure 10. Stress Block of a rectangular reinforced concrete section [13]

2.5.2 Stress-Strain of Steel

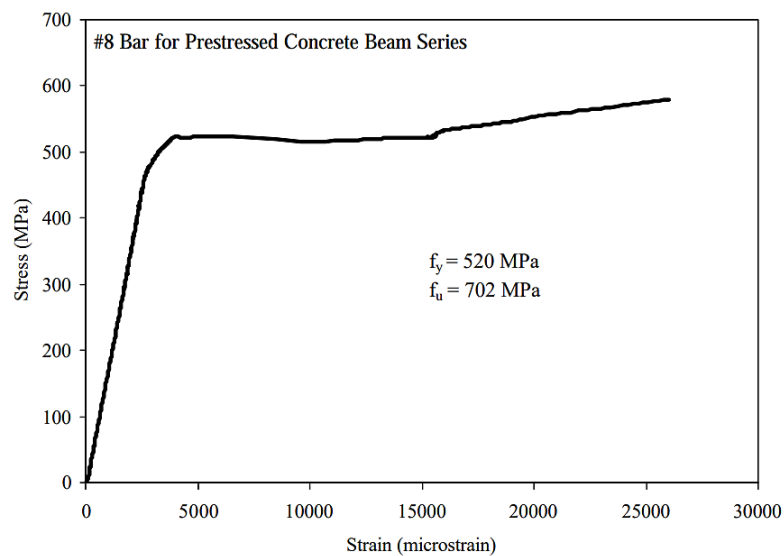


Figure 11. Stress-Strain curve for #8 bar (25.4 mm diameter) [9]

The stress-strain curve of steel bars is generated from the Tensile Strength Test. This test is conducted in the Universal Testing Machine (UTM). The steel bar is pulled from both ends with an increasing load until it reaches the ultimate stress.

When the ultimate stress is reached, necking will keep forming until it breaks.

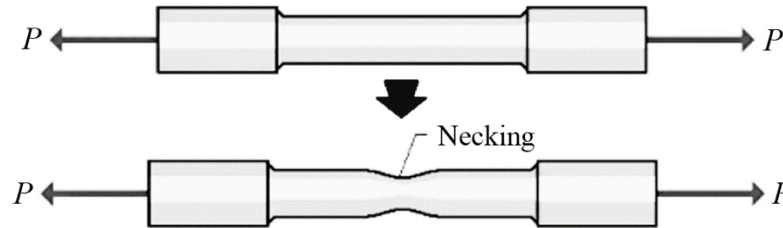


Figure 12. Necking forming in the steel bar [14]

Finally, the stress-strain graph is generated from the data gathered during the tensile test.

The relationship between stress and strain in steel differentiates according to the bar diameter.

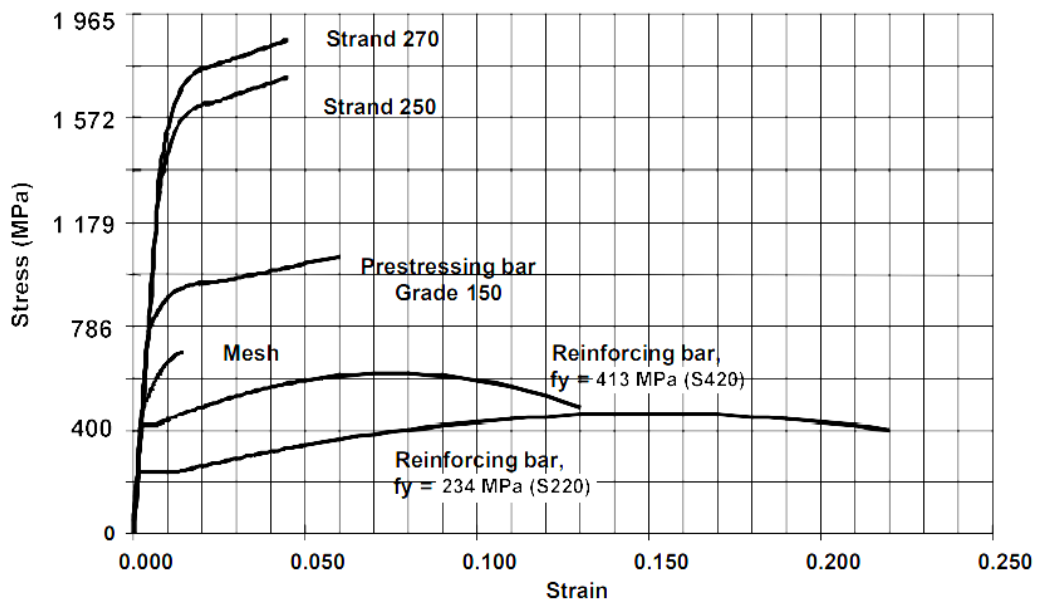


Figure 13. Stress-Strain curve for several types of reinforcing steel [9]

The stress-strain relationship is also different for cold-worked and hot-rolled steel bars. Cold-worked steel bars have high strength but lower ductility than the widely used hot-rolled steel bars (*Figure 14*).

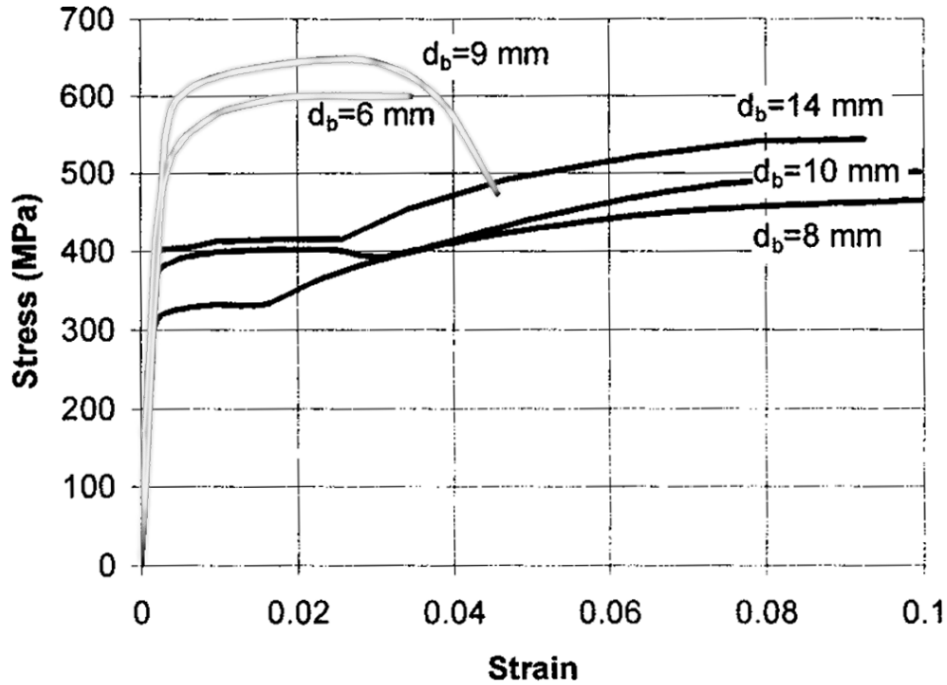


Figure 14. Stress-strain curve for steel bars with different diameters. The 6 mm and 9 mm curves represent cold-worked steel bars [15].

The ideal stress-strain curve which is widely used in civil engineering is shown in *Figure 15*. Each region represents the phases that the material, in this case, steel, goes through.

- a) In **Region AB**, steel is linearly elastic. The stress-strain relationship and material properties are predictable and easily expressible by formula expressions. The strain is elastic; thus, the steel specimen will revert to its initial dimensions when unloaded. For $\epsilon_s \leq \epsilon_y$ and Modulus of Elasticity, $E_s = 210 \text{ GPa}$ [16]:

$$\epsilon_s = \frac{f_s}{E_s} \Rightarrow f_s = E_s * \epsilon_s \quad (\text{Equation 3})$$

- b) **Region BC** is the yield point. Steel has reached its elastic limit and it is beginning its plastic phase. From this point on, the steel capacity is considered as failed and not suitable for further use. For $\varepsilon_y \leq \varepsilon_s \leq \varepsilon_s$:

$$f_s = f_y \quad (\text{Equation 4})$$

- c) In **Region CD**, steel is non-linearly plastic. The stress-strain relationship is expressible by experimental data and the strain in plastic. When unloaded, the steel specimen will not revert to its initial dimensions. For $\varepsilon_{sh} \leq \varepsilon_s \leq \varepsilon_u$:

$$f_s = f_y * \left(\frac{m * (\varepsilon_s - \varepsilon_{sh}) + 2}{60 * (\varepsilon_s - \varepsilon_{sh}) + 2} + \frac{(\varepsilon_s - \varepsilon_{sh}) * (60 - m)}{2 * (30 * r + 1)^2} \right) \quad (\text{Equation 5})$$

Where:

$$m = \frac{\left(\frac{f_{su}}{f_y} \right) * (30 * r + 1)^2 - 60 * r - 1}{15 * r^2} \quad (\text{Equation 6})$$

$$r = \varepsilon_{su} - \varepsilon_{sh} \quad (\text{Equation 7})$$

- d) **Point D** is the Ultimate Strength Limit. Steel has reached its maximal strain and cannot “stretch” further. ASTM A706 Standard [17] demands:

$$\frac{f_{su}}{f_{y,actual}} > 1,25 \quad (\text{Equation 8})$$

- e) **Region DE** is the final region. Necking will start forming at point D (*Figure 12*) and finally, the steel specimen will rupture at point E. For $\varepsilon_s > \varepsilon_{su}$:

$$f_s = 0 \quad (\text{Equation 9})$$

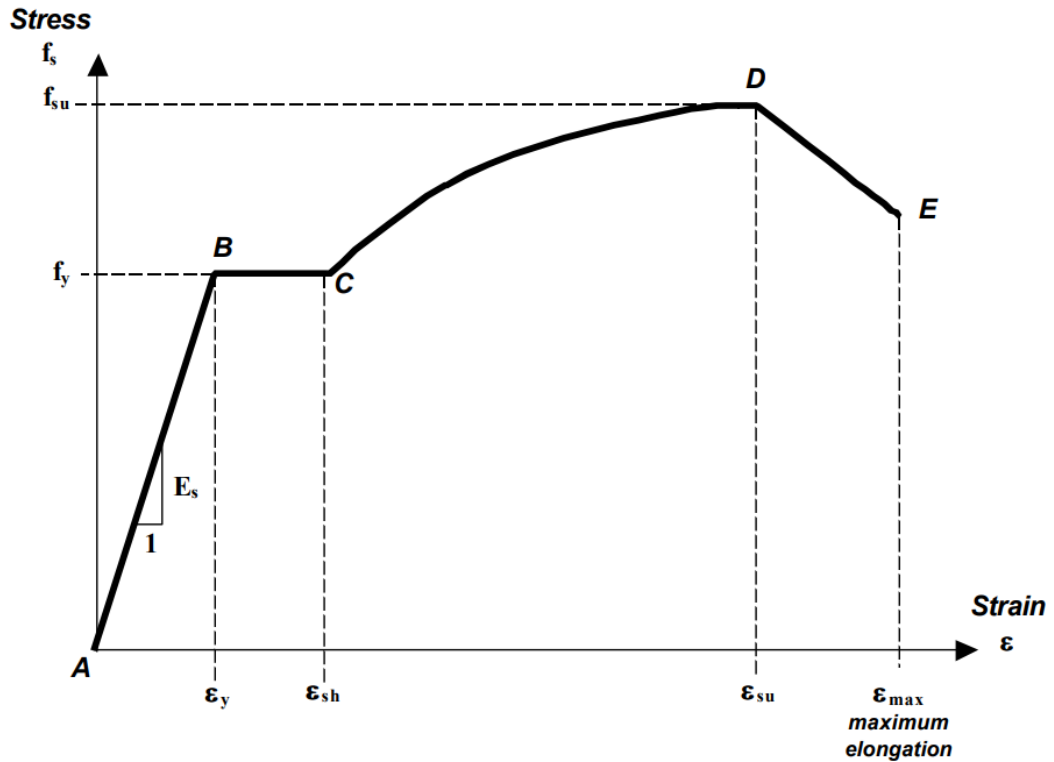


Figure 15. Idealised Stress-Strain Curve for Reinforcing Steel [9]

2.5.3 Stress-Strain of Concrete

The stress-strain relationship for concrete is obtained by the Concrete Compression Test. The test is conducted 28 days after the concrete is set, due to it reaching 99% of its strength. A cylindrical (150x300 mm) or cubic (150x150x150 mm) sample is placed inside the Compression Test Machine and is placed under a constantly increasing load until it fails [18]. Due to the ease of drilling on-site and flexibility, the cylindrical shape is the most widely used for the specimen. The cylindrical specimen's strength is usually 10%-20% less than the equivalent cube specimen.

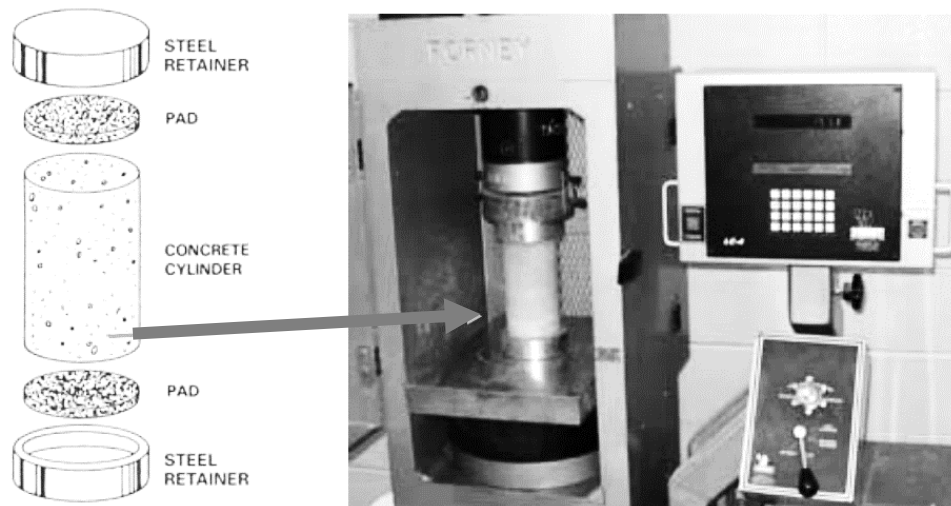


Figure 16. Compression Test Machine [19]

The stress-strain curve for unconfined concrete has three regions, as shown in *Figure 17*, the linear ascending curve that represents the elastic phase, the non-linear ascending curve that represents the plastic phase and the peak point and descending curve that represents failure [20].

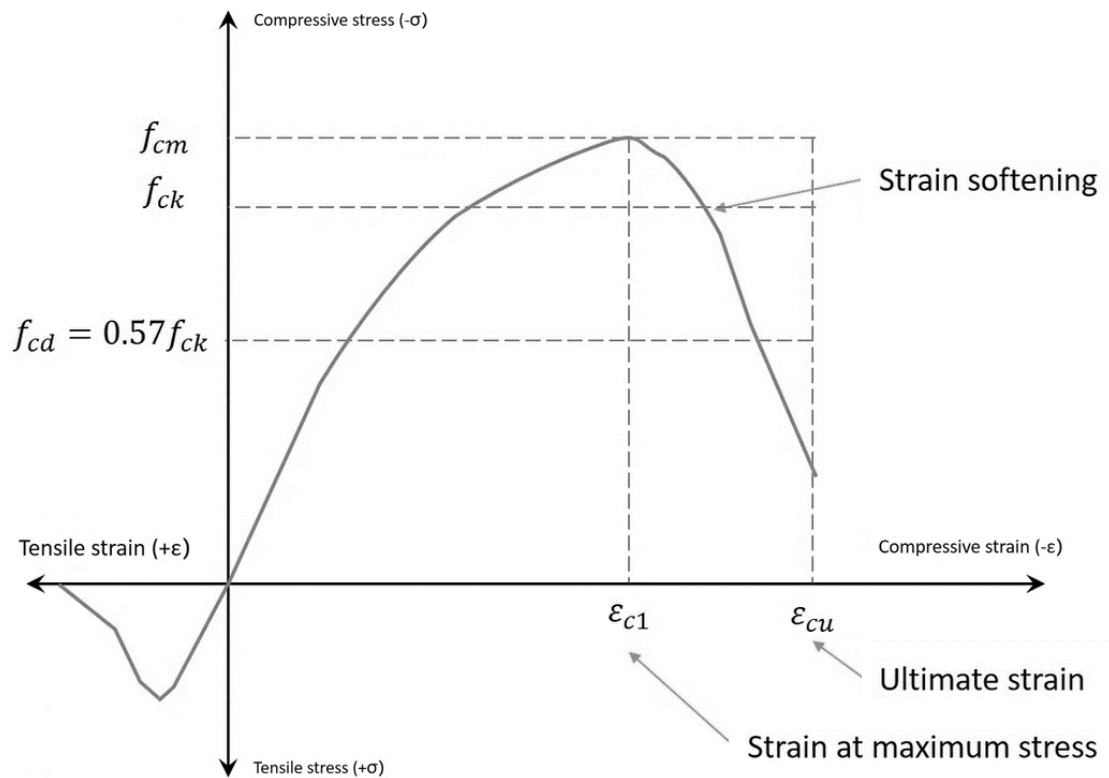


Figure 17. Stress-Strain curve for Unconfined Concrete [21]

CHAPTER 3

METHODOLOGY

3.1 Global and Local Levels

To analyse the safety of a structure, we need to consider the Local \rightarrow Global levels relationship: Material \rightarrow Section \rightarrow Member/Connection \rightarrow System [2].

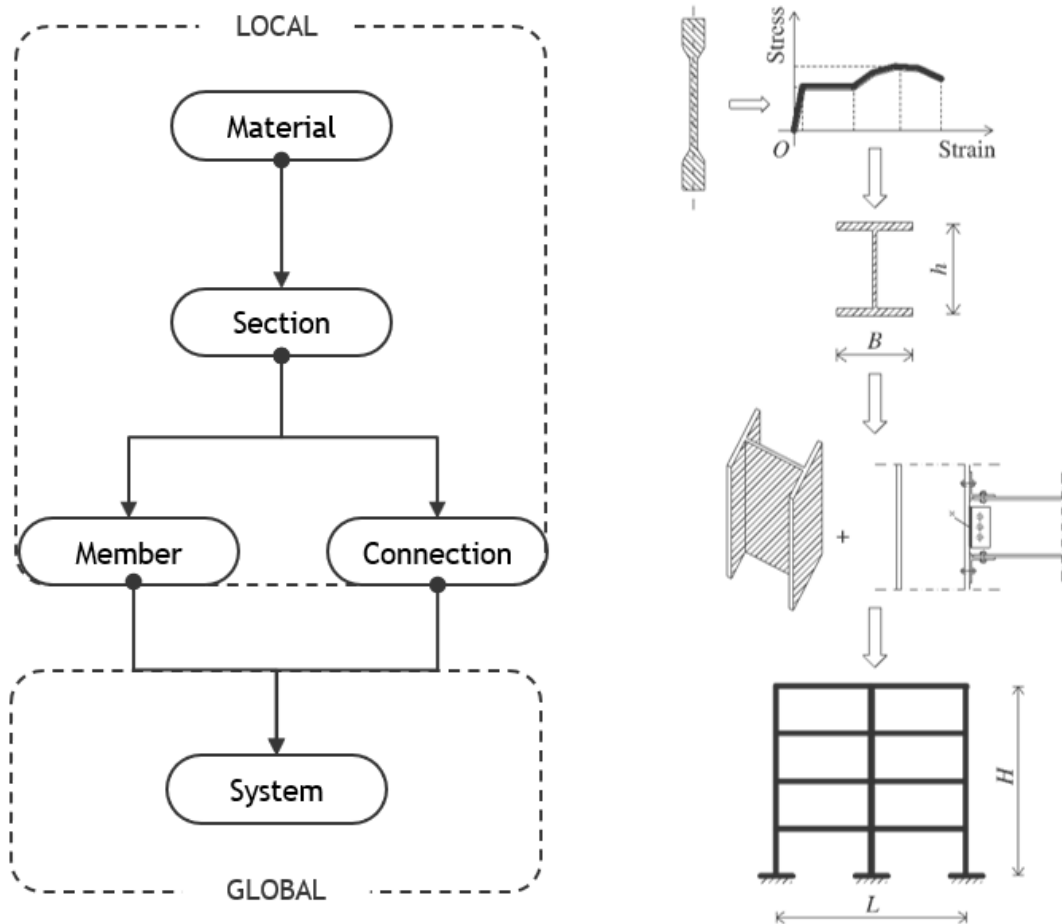


Figure 18. Global and Local Levels Hierarchy [2]

Starting with the first level of the hierarchy, material, we need to understand and predict the behaviour of concrete from its stress-strain relationship. From the curve, the elastic limit where concrete transitions from elastic to plastic phases can be

determined. The plastic phase is non-linear and involves cracking and crushing of concrete.

Moving to the next section level, the moment-curvature relationship describes how the cross-section deforms in response to applied moments. It determines the location and rotation of plastic hinges, which are the regions where concrete has cracked (determined from the stress-strain relationship) and steel has yielded. The plastic hinges indicate the loss of stiffness and strength of the section.

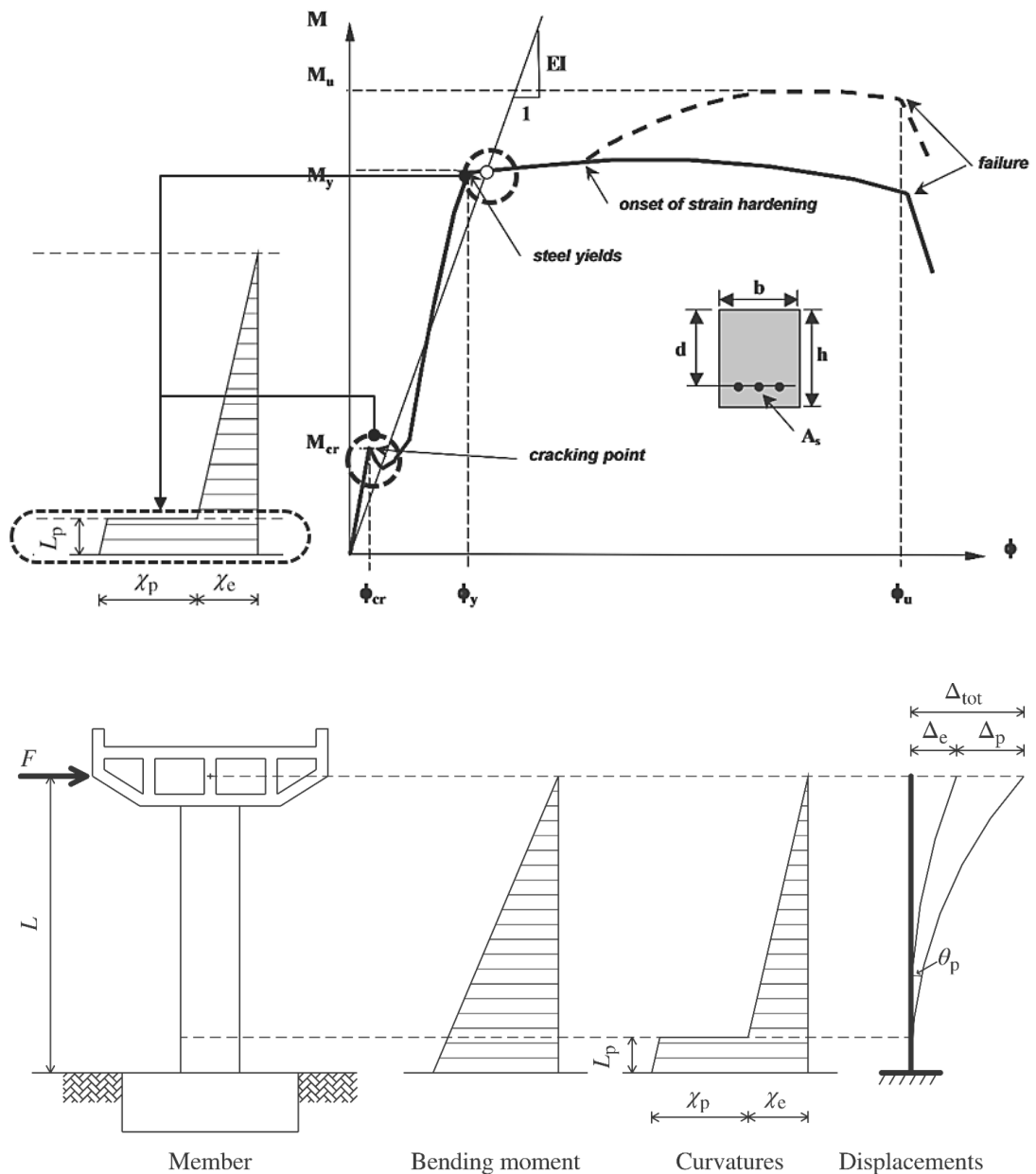


Figure 19. Locating plastic hinges from moment-curvature [2], [9]

The next level is the member/connection level. As previously stated, concrete will undergo elastic deformation, reach its elastic limit, and then go to plastic deformation. This plastic deformation is concentrated in plastic hinges, which are critical points of failure. The plastic hinges affect the ductility and stability of the member and connection, as well as their energy dissipation capacity.

Finally, at the system level, the non-linear static pushover analysis of roof displacement versus base shear is performed. This displacement-based method considers the non-linear behaviour of the material for more realistic results. It helps evaluate the global performance of the system under different load levels and patterns.

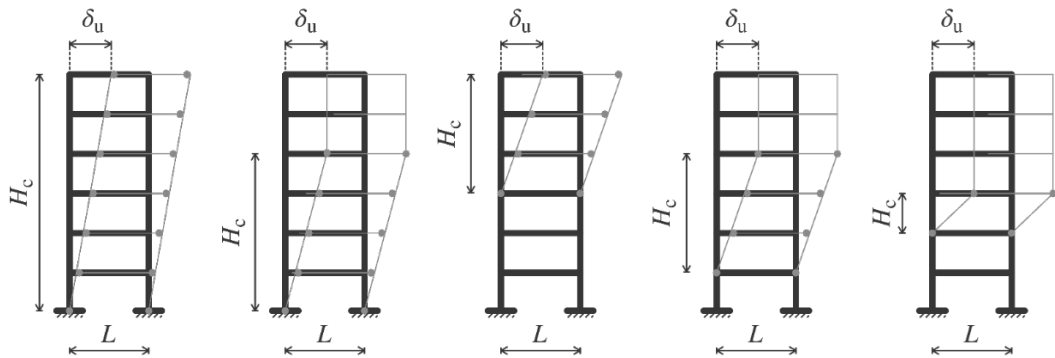


Figure 20. Typical plastic mechanisms for moment-resisting frames

3.2 Confined Concrete Models

The stress-strain curve of concrete is influenced by numerous components, making it impossible to define a single curve for each case, especially for the non-linear phase. Thus, researchers have proposed different concrete models that describe the behaviour of concrete using empirical equations.

Table 2. Peak stress and strain for some concrete models [1]

Researcher	Peak stress, (f_{cc})	Peak strain, (ϵ_{cc})
Sheikh and Uzumeri	$K_s 0.85 f_{uc}$ $K_s = 1 + \frac{B'^2}{140 P_{occ}} \left[\left(1 - \frac{n C'^2}{5.5 B'^2} \right) \left(1 - \frac{s}{2 B'} \right)^2 \right] \sqrt{p_s f_y}$	$80 K_s f_{uc} 10^{-6}$
Fafitis and Shah	$f_{uc} + \left[1.15 + \left(\frac{3048}{f_{uc}} \right) \right] f_l$	$1.027 10^{-7} f_{uc} + 0.0296 \left(\frac{f_l}{f_{cc}} \right) + 0.00195$
Mander et al.	$f_{uc} \left[2.254 \sqrt{1 + 7.94 \left(\frac{f_l}{f_{uc}} \right)} - 2 \left(\frac{f_l}{f_{uc}} \right) - 1.254 \right]$	$\epsilon_{co} \left[1 + 5 \left(\frac{f_{cc}}{f_{uc}} - 1 \right) \right]$
Yong et al.	$\left[1 + 0.0091 \left(1 - \left(\frac{0.245 s}{B} \right) \left(p_s + \frac{n d'_{st}}{B s d_s} p_t \right) \left(\frac{f_{yh}}{\sqrt{f_{uc}}} \right) \right) \right] f_{uc}$	$\frac{0.00265 + 0.0035 \left(1 - \frac{0.734 s}{B} \right) (p_s f_{yh})^{\frac{2}{3}}}{\sqrt{f_{uc}}}$
Saatçioğlu et al.	$f_{uc} + 6.7 (f_l)^{-0.17} f_l$	$\epsilon_{co} [1 + 5 K]$ $K = 6.7 (f_l)^{-0.17} \frac{f_l}{f_{uc}}$
El-Dash & Ahmad	$f_{uc} + \left[5.1 \left(\frac{f_{uc}}{f_{yh}} \right)^{0.5} \left(\frac{d'_{st}}{p_s} \right)^{0.25} \right] f_l$ $f_l = 0.5 p_s f_{yh} \left(1 - \sqrt{\frac{s}{1.25 d_s}} \right)$	$\epsilon_{co} + \left[\frac{66}{\left(\frac{s}{d'_{st}} \right) f_{uc}^{1.7}} \right] \frac{f_l}{f_{uc}}$
Cusson and Paultre	$f_{uc} + 2.1 \left(\frac{f_l}{f_{uc}} \right)^{0.7}$	$\epsilon_{co} + 0.21 \left(\frac{f_l}{f_{uc}} \right)^{1.7}$
Mansure et al.	$f_{uc} \left[1 + 0.6 \left(\frac{p_s f_y}{f_{uc}} \right)^{1.23} \right]$	$\epsilon_{co} \left[1 + 2.6 \left(\frac{p_s f_y}{f_{uc}} \right)^{0.8} \right]$
Hoshikum a et al.	$f_{uc} \left[1 + 0.73 \left(\frac{p_s f_y}{f_{uc}} \right) \right]$	$0.00245 + 0.0122 \left(\frac{p_s f_y}{f_{uc}} \right)$
Assa et al.	$f_{uc} \left[1 + 3.36 \frac{f_l}{f_{uc}} \right]$	$\epsilon_{co} \left[1 + 21.5 \frac{f_l}{f_{uc}} \right]$

3.2.1 Modified Kent-Park Model

The Modified Kent-Park Model is based on the original Kent-Park Model by taking into consideration the change in concrete strength due to the confinement. The maximum stress and strain are at point B [9].

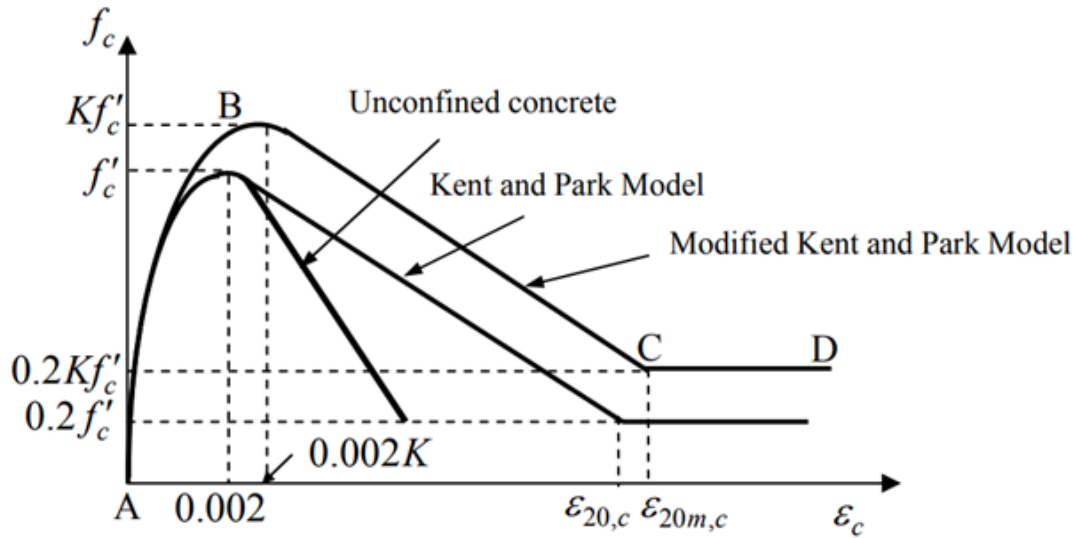


Figure 21. Stress-Strain Relationship for Concrete proposed by Kent and Park [22]

$$K = 1 + \frac{\rho_s f_{yh}}{f'_c} \quad (\text{Equation 10})$$

f_{yh} = yield strength of steel hoops

The stress block parameters for this model are demonstrated in Figure 22.

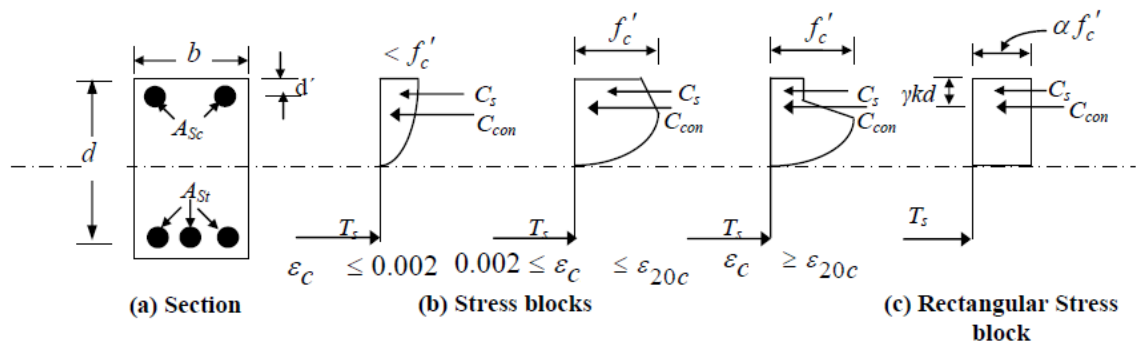


Figure 22. Stress Block for the Modified Kent-Park Model [22]

- a) **Region AB**, where $\epsilon_c \leq 0,002$. The unconfined and confined curves are the same in the original model. The maximum stress at B is taken from the cylinder's compressive strength test.

$$f_c = K * f'_c * \left(\frac{2\varepsilon_c}{0.002K} - \left(\frac{\varepsilon_c}{0.002K} \right)^2 \right) \quad (\text{Equation 11})$$

$$\alpha = \frac{\varepsilon_c}{0.002K} * \left(1 - \frac{\varepsilon_c}{0.006K} \right) \quad (\text{Equation 12})$$

$$\gamma = 1 - \frac{\frac{2}{3} - \left(\frac{\varepsilon_c}{0.008K} \right)}{1 - \left(\frac{\varepsilon_c}{0.006K} \right)} \quad (\text{Equation 13})$$

b) **Region BC**, where $0,002K \leq \varepsilon_c \leq \varepsilon_{20m,c}$.

$$f_c = K * f'_c * (1 - Z_m * (\varepsilon_c - 0.002K)) \geq 0.2 * K * f'_c \quad (\text{Equation 14})$$

$$\alpha = \frac{1}{\varepsilon_c} * \left(\frac{0.004K}{3} + (\varepsilon_c - 0.002K) - \frac{Z}{2} * (0.002K)^2 \right) \quad (\text{Equation 15})$$

$$\gamma = 1 - \frac{1}{\varepsilon_c} * \left(\frac{\left(\frac{\varepsilon_c^2}{2} - \frac{(0.002K)^2}{12} \right) - Z * \left(\frac{\varepsilon_c^3}{3} - 0.001K * \varepsilon_c^2 + \frac{(0.002K)^3}{6} \right)}{\left(\varepsilon_c - \frac{0.002K}{3} \right) - Z * \left(\frac{\varepsilon_c^2}{2} - 0.002K * \varepsilon_c + \frac{(0.002K)^2}{2} \right)} \right) \quad (\text{Equation 16})$$

Where:

$$Z = \frac{0,5}{\varepsilon_{50u} + \varepsilon_{50h} - 0.002K} \quad (\text{Equation 17})$$

The strain for each critical point is:

$$\varepsilon_{50u} = \frac{3 + 0.29f'_c}{145f'_c - 1,000} \quad (\text{Equation 18})$$

$$\varepsilon_{50h} = \frac{3}{4} \rho_s \sqrt{\frac{b''}{s_h}} \quad (\text{Equation 19})$$

3.2.2 Saatçioğlu-Razvi Model

Saatçioğlu and Razvi proposed a model based on uniform confinement pressure caused by transverse reinforcement. This model can be applied to both circular and rectangular sections. This model consists of a parabolic rising curve and a linear decreasing curve up to 20% of the concrete's strength [4].

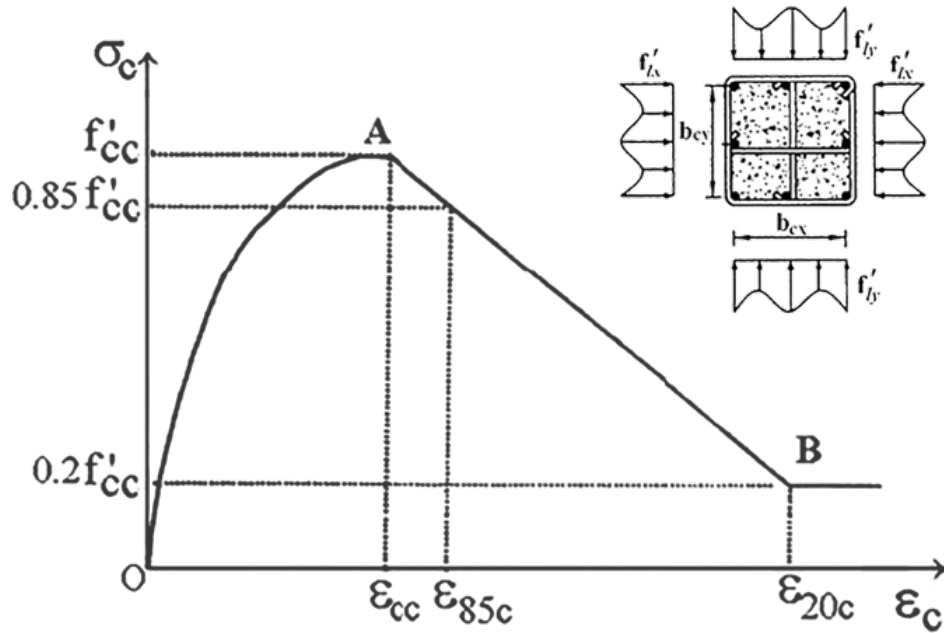


Figure 24. Stress-Strain Relationship of Confined Concrete proposed by Saatçioğlu and Razvi [4]

The parabolic curve can be expressed by the following equation:

$$f_c = f'_{cc} * \left(2 * \left(\frac{\epsilon_c}{\epsilon_{cc}} \right) - \left(\frac{\epsilon_c}{\epsilon_{cc}} \right)^2 \right)^{\frac{1}{1+2K}} \quad (\text{Equation 24})$$

Where:

$$f'_{cc} = f_{co} + k_1 * f'_l \quad (\text{Equation 25})$$

$$\epsilon_{cc} = \epsilon_{co} * (1 + 5K) \quad (\text{Equation 26})$$

$$\varepsilon_{co} = 0.002 \quad (\text{Equation 27})$$

$$\varepsilon_{20c} = 0.2f'_{cc} \quad (\text{Equation 28})$$

$$K = \frac{k_1 * f'_l}{f_{co}} \quad (\text{Equation 29})$$

$$k_1 = 6.7 * (f'_l)^{-0.17} \quad (\text{Equation 30})$$

$$f_l = k_2 * f_l \quad (\text{Equation 31})$$

$$k_2 = 0.26 \sqrt{\left(\frac{b_c}{s}\right) * \left(\frac{b_c}{s_l}\right) * \left(\frac{1}{f_l}\right)} \quad (\text{Equation 32})$$

For circular sections:

$$f_l = \frac{2A_{sh} * f_{yh}}{d_c * s} \quad (\text{Equation 33})$$

For rectangular sections:

$$f_l = \frac{\sum 2A_{sh} * f_{yh} * \sin \alpha}{b_c * s} \quad (\text{Equation 34})$$

For square sections:

$$f_l = \frac{f'_{lx} * b_{cx} + f'_{ly} * b_{cy}}{b_{cx} + b_{cy}} \quad (\text{Equation 35})$$

Where:

f_{co} – unconfined concrete compressive strength

f'_l – effective lateral pressure

f'_{lx} – effective lateral pressure perpendicular to b_{cx}

f'_{ly} – effective lateral pressure perpendicular to b_{cy}

α – angle of stirrup with b_c

b_c, b_{cx}, b_{cy} – core dimensions from stirrup centre to stirrup centre

s – distance between transverse reinforcement

s_l – distance between longitudinal reinforcement

$k_2 = 1$ for circular and rectangular sections with small
– spaced transverse reinforcement

The descending linear curve can be expressed from the strain corresponding to 85% of the concrete's strength:

$$\epsilon_{85c} = 260\rho_{sh} * \epsilon_{cc} + \epsilon_{85u} \quad (\text{Equation 36})$$

$$\rho_{sh} = \frac{\sum A_{sh}}{s(b_{cx} + b_{cy})} \quad (\text{Equation 37})$$

Where:

$$\epsilon_{85c} = 0.85f'_{cc} \quad (\text{Equation 38})$$

ρ_{sh} – volumetric ratio of transverse reinforcement

A_{sh} – cross – sectional area of transverse reinforcement

3.2.3 Mander Model

One of the most widely used confined concrete models is the Mander model. It is used as the default model in a lot of structural engineering software, such as SAP2000 [7]. Mander proposed a unified stress-strain model that includes both circular and rectangular confined concrete sections. The stress-strain curve is derived from Popovics' Equation [23], while the confinement coefficient is like the approach of Sheikh and Uzumeri [24]. This model incorporates the effect of arching pressure as the source of confining stress.

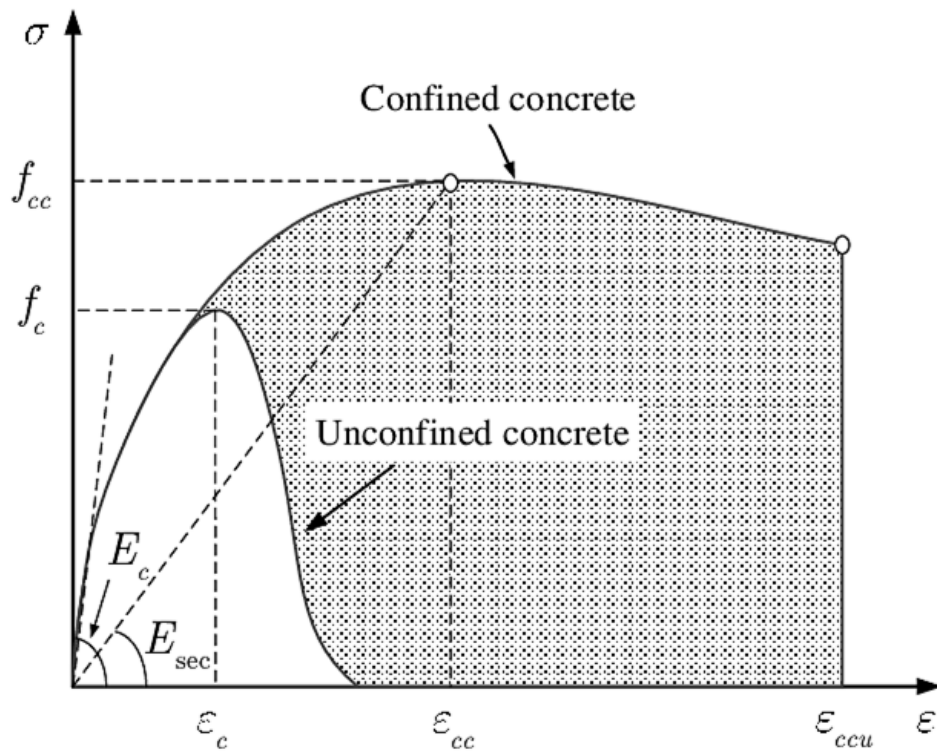


Figure 25. Stress-Strain Relationship of Concrete proposed by Mander [25]

The effective cylinder compressive strength of confined concrete is 0.8 times the cube compressive strength of confined concrete. The thickness and spacing of the transverse reinforcement affect the confining stress and the effective lateral pressure determines the peak cylinder strength. When $f_l = 0 \rightarrow f'_{cc} = f'_c$.

$$f'_{cc} = f'_c * \left(2.254 * \sqrt{1 + 7.94 * \frac{f'_l}{f'_c}} - 2 * \frac{f'_l}{f'_c} - 1.254 \right) \quad (\text{Equation 39})$$

$$f_c = \frac{f'_{cc} * x * r}{r - 1 + x'} \quad (\text{Equation 40})$$

$$f'_c = 0.8f_{ck} \quad (\text{Equation 41})$$

Where:

$$x = \frac{\varepsilon_c}{\varepsilon_{cc}} \quad (\text{Equation 42})$$

$$\varepsilon_{cc} = 0.002 * \left(1 + 5 * \left(\frac{f'_{cc}}{f'_c} - 1 \right) \right) \quad (\text{Equation 43})$$

$$r = \frac{E_c}{E_c - E_{sec}} \quad (\text{Equation 44})$$

$$E_c = 5000\sqrt{f'_c} \quad (\text{Equation 45})$$

$$E_{sec} = \frac{f'_{cc}}{\varepsilon_{cc}} \quad (\text{Equation 46})$$

f'_c – cylinder compressive strength of unconfined concrete

f'_{cc} – cylinder strength of confined concrete

f'_l – confining stress

When experiencing repeated load cycles, the unloading curves follow the same pattern as the monotonic curve until the maximum stress, but the unloading modulus is modified by two coefficients that depend on the stress, f_{un} , and strain, ε_{un} , at the unloading point [26].

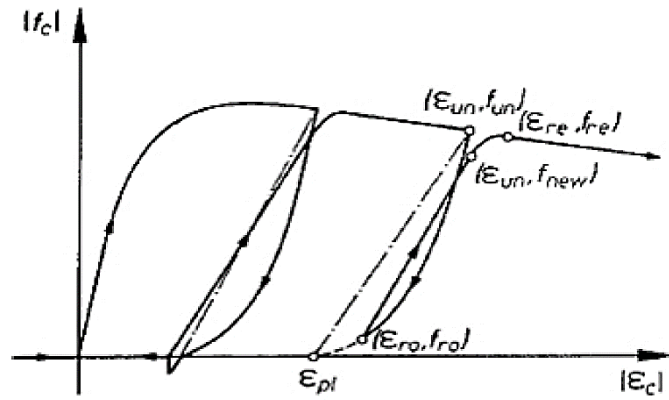


Figure 26. Mander model response under load cycles [26]

3.3 Moment-Curvature Relationship

In the analysis of reinforced concrete structures, the deformation of its members is an important factor to consider. The displacement of a member reflects its ability to resist stresses caused by external loads. Therefore, the displacement must be determined accurately and efficiently. Moment-curvature relationship describes how the cross-section deforms in response to applied forces.

A simply supported beam with a point load P applied is shown in Figure 27. The deformation shape of the beam can be expressed as the function $y = f(x)$, as illustrated in Figure 28.

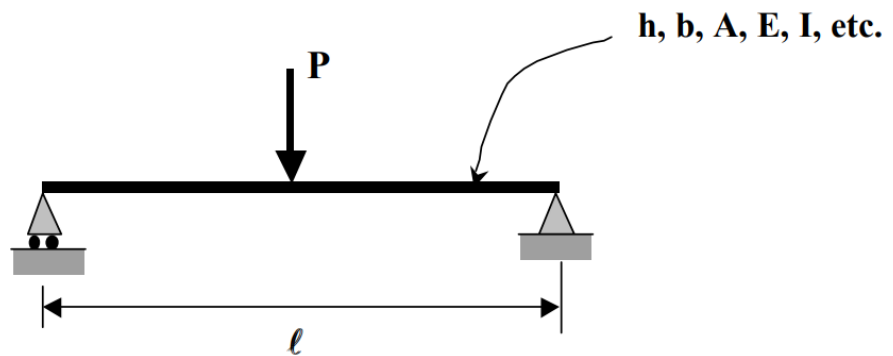


Figure 27. Beam Member with a specific length and section [9]

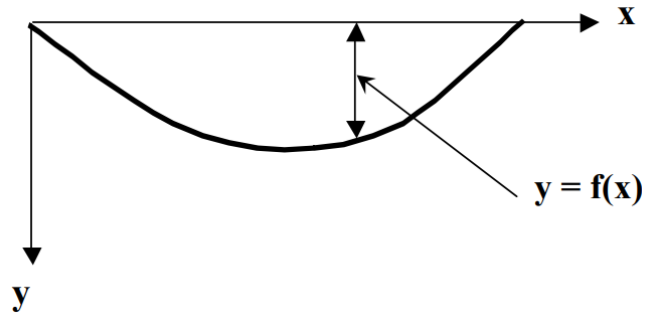


Figure 28. Deflection curve of a beam under an axial load [9]

A small section from the member is taken and a moment M is applied along the neutral axis of its cross-section.

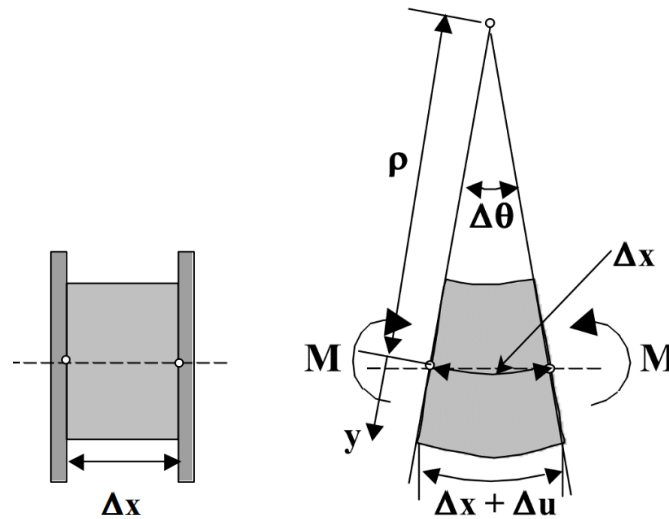


Figure 29. Small section taken from a simply supported beam [9]

The distance of the neutral axis to the centre of rotation is:

$$\rho = \frac{\Delta x}{\Delta \theta} \text{ for } \Delta \theta \ll \ll \quad (\text{Equation 47})$$

The length of the fibre at any distance, y , is:

$$\Delta x + \Delta u = \Delta \theta * (\rho + y)$$

$$\Delta u = \Delta \theta * y \quad (\text{Equation 48})$$

$$\varepsilon = \frac{du}{dx} = y * \frac{d\theta}{dx} = y * \phi \quad (\text{Equation 49})$$

Considering the linearly elastic region of concrete, Hook's Law is eligible.

$$\sigma = E * \varepsilon = E * y * \phi \quad (\text{Equation 50})$$

The moment in the section is:

$$M = \int_A \sigma * y * dy = \int_A E * y^2 * \phi * dy = \phi * E * \int_A y^2 * dy$$

$$M = \phi * E * I \quad (\text{Equation 51})$$

Consequently, the curvature is the ratio of the moment to the section properties.

$$\phi = \frac{1}{\kappa} = \frac{M}{EI} \quad (\text{Equation 52})$$

From *Figure 28*, the elastic deformation curve can be expressed as:

$$EI \frac{d^4 y}{dx^4} = p(x) \quad (\text{Equation 53})$$

Where:

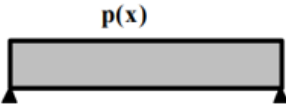
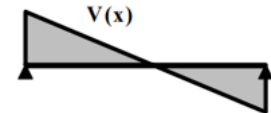
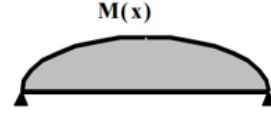

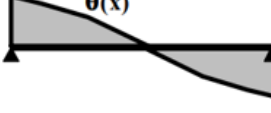

y = deflection of the member at x

x = position of the section

$p(x)$ = applied load

By integrating the equation successively, *Shear*, $V \rightarrow$ *Moment*, $M \rightarrow$ *Curvature*, $\phi \rightarrow$ *Rotation*, $\theta \rightarrow$ *Deflection*, δ can be obtained (Table 3). This linear relationship is valid only for the elastic range of concrete.

Table 3. $P \rightarrow V \rightarrow M \rightarrow \phi \rightarrow \theta \rightarrow \delta$ Relationship [9]

Load	$p(x)$	
Shear	$V(x) = \int p(x) d(x)$	
Moment	$M(x) = \int V(x) d(x)$	
Curvature	$\phi(x) = \frac{M(x)}{EI}$	
Rotation	$\theta(x) = \int \phi(x) d(x)$	
Deflection	$\delta(x) = \int \theta(x) d(x)$	

The Moment-Curvature relationship is analysed at the section system level, which means that only the section properties, such as the geometry, material, and reinforcement, are required to be known to perform the analysis.

3.3.1 Calculating Moment-Curvature according to Kent-Park Model

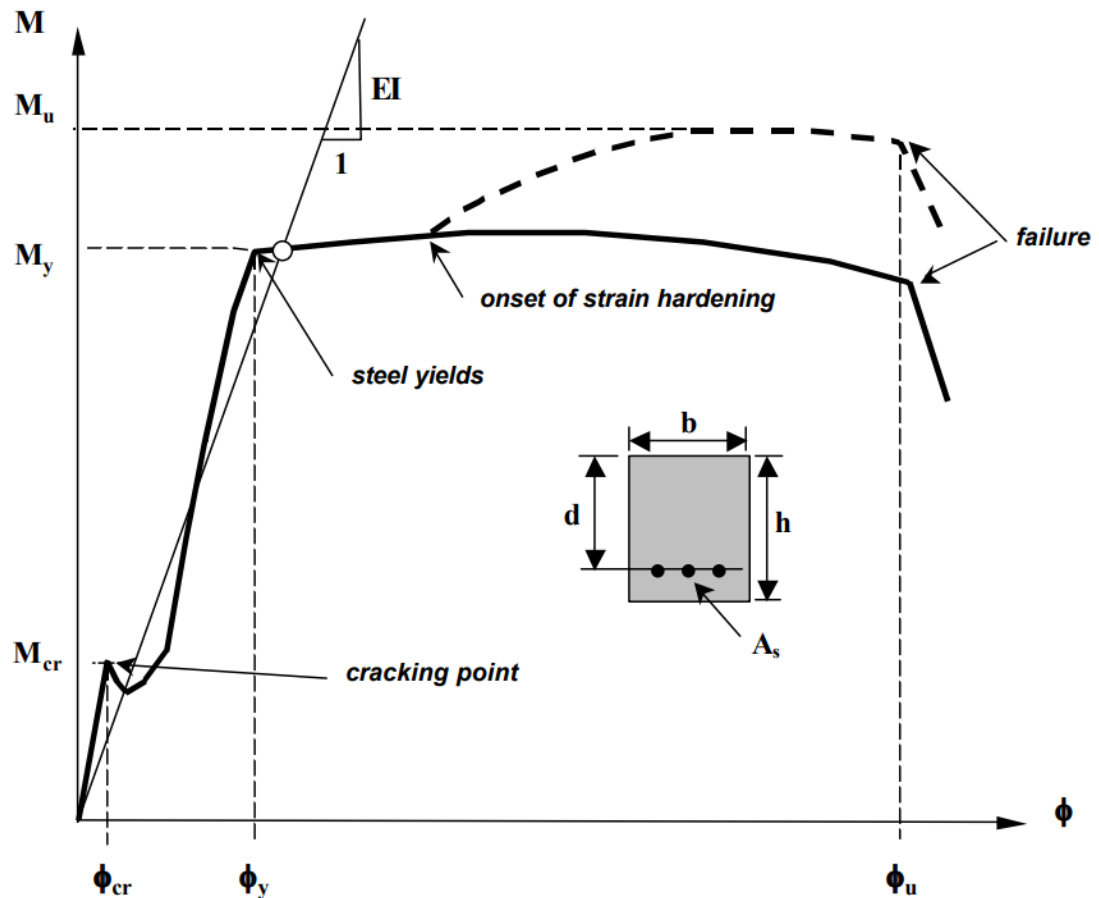


Figure 30. Moment-Curvature curve of an unconfined concrete beam [9]

The calculation of the moment-curvature relationship of unconfined concrete sections according to the Kent-Park model is explained in detail. All the phases of the material behaviour, such as concrete cracking, steel yielding and ultimate failure, are considered.

I. Uncracked Stiffness:

In the first region, the relationship is linearly elastic. The procedure of calculating the curvature begins with transforming the area of the cross-section to an equivalent concrete area by multiplying the variables by the coefficient of equivalency.

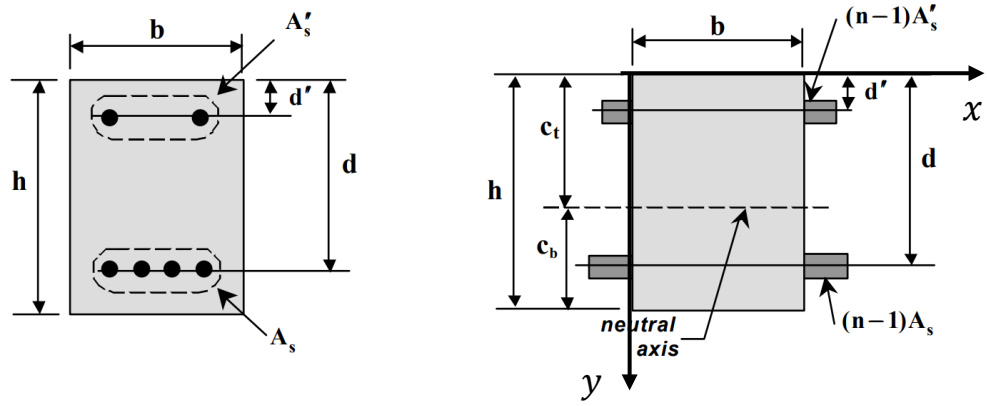


Figure 31. Transformation of the reinforced concrete cross-section to an equivalent concrete section [9]

$$n = \frac{E_s}{E_c} \quad (\text{Equation 54})$$

Where:

$$E_s = 200 \text{ GPa} = 200,000 \text{ MPa} \quad (\text{Equation 55})$$

$$E_c = 4,700 * \sqrt{f'_c} \text{ (MPa)} \quad (\text{Equation 56})$$

The distance of the neutral axis to the top fibre is denoted with c_t .

$$c_t = \frac{\sum(y * A)}{\sum A} = \frac{b * h * \frac{h}{2} + (n + 1) * A_s * d + (n - 1) * A'_s * d'}{b * h + (n - 1) * A_s + (n - 1) * A'_s} \quad (\text{Equation 57})$$

And the remaining distance is:

$$c_b = h - c_t \quad (\text{Equation 58})$$

The moment of Inertia of the section is calculated as follows:

$$I = \sum (I_0 + A * d_0) \quad (\text{Equation 59})$$

$$I = \frac{1}{12} * b * h^3 + b * h * \left(\frac{h}{2} - c_t\right)^2 + (n - 1) * (A_s * (d - c_t)^2 + A'_s * (c_t - d')^2)$$

(Equation 60)

Where:

$I_0 =$ Moment of Inertia of the specific section

$d_0 =$ the distance from the neutral axis of the specific section to c_b

II. Cracking Point:

The first region concludes with the cracking point in which concrete reaches its elastic limit. The compressive stress can be analytically calculated or taken from a compressive cylinder strength test.

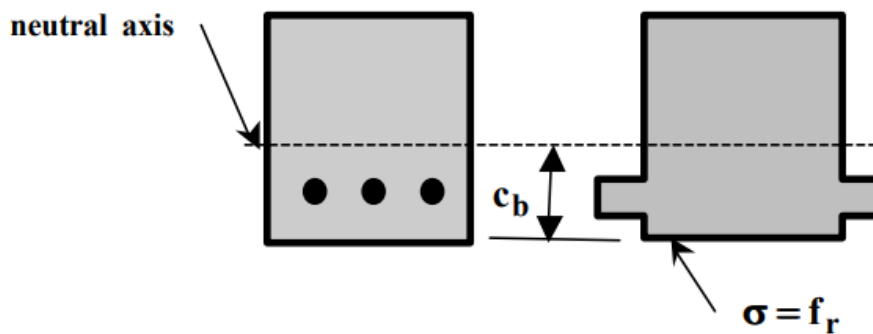


Figure 32. The stress block at the cracking point [9]

The maximum amount of stress, which in this case is the tensile stress, that concrete can withstand is calculated with the Modulus of Rupture [27]:

$$f_r = 0,7 * \sqrt{f'_c} * \lambda$$

(Equation 61)

Where: $\lambda = 1,00$ for normal weight concrete.

At this point, the stress is equal to that of the modulus of rupture.

$$\sigma_{cr} = \frac{M_{cr} * c_b}{I} = f_r \quad (\text{Equation 62})$$

Finally, the cracking moment and curvature at the cracking point are:

$$M_{cr} = \frac{f_r * I}{c_b} \quad (\text{Equation 63})$$

$$\phi_{cr} = \frac{\epsilon_r}{c_b} \quad (\text{Equation 64})$$

From Hooke's Law:

$$f_r = \epsilon_r * E_c \quad (\text{Equation 65})$$

$$\epsilon_c = \phi_{cr} * c_t \quad (\text{Equation 66})$$

III. Yielding Point:

The yielding point is the point where steel yields, thus $\epsilon_s = \epsilon_y$.

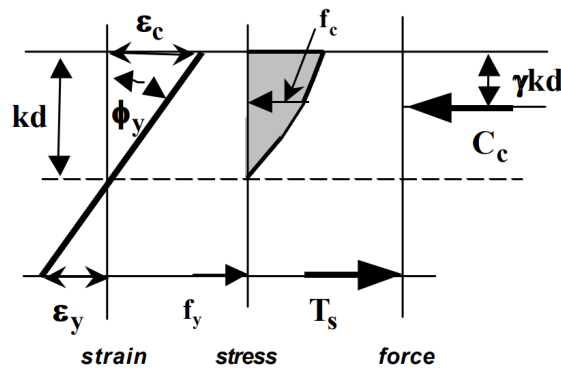


Figure 33. The stress block at the yielding point [9]

$$\sum F_x = 0$$

$$T_s = C_c$$

$$A_s * f_y = \alpha * f'_c * b * k * d$$

From strain compatibility:

$$\frac{\epsilon_c + \epsilon_y}{d} = \frac{\epsilon_c}{k * d} \Rightarrow k = \frac{\epsilon_c}{\epsilon_c + \epsilon_y}$$

$$\Rightarrow A_s * f_y = \alpha * f'_c * b * \frac{\epsilon_c}{\epsilon_c + \epsilon_y} * d$$

Finally, the yielding moment and curvature at the yielding point are:

$$M_y = A_s * f_y * d * (1 - k * \gamma) \quad (\text{Equation 67})$$

$$\phi_y = \frac{\epsilon_c}{k * d} \quad (\text{Equation 68})$$

IV. Ultimate Load:

The ultimate load point is the point where concrete reaches its ultimate strain and fails, thus $\epsilon_c = \epsilon_{cu}$.

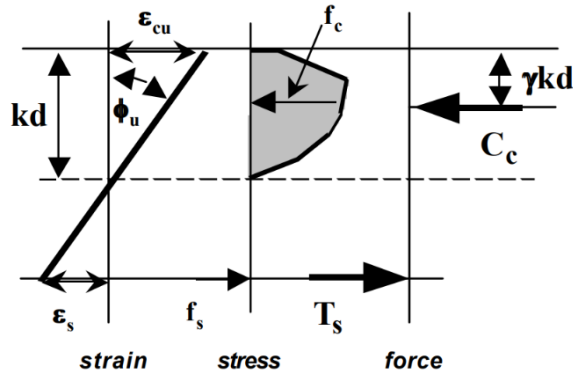


Figure 34. The stress block at the ultimate load point [9]

$$\sum F_x = 0$$

$$T_s = C_c$$

$$A_s * f_y = \alpha * f'_c * b * k * d$$

From strain compatibility:

$$\frac{\epsilon_{cu} + \epsilon_s}{d} = \frac{\epsilon_{cu}}{k * d} \Rightarrow k = \frac{\epsilon_{cu}}{\epsilon_{cu} + \epsilon_s}$$

$$\Rightarrow A_s * f_s = \alpha * f'_c * b * \frac{\epsilon_{cu}}{\epsilon_{cu} + \epsilon_s} * d$$

Finally, the ultimate moment and curvature at this point are:

$$M_u = A_s * f_s * d * (1 - k * \gamma) \quad (\text{Equation 69})$$

$$\phi_u = \frac{\epsilon_{cu}}{k * d} \quad (\text{Equation 70})$$

3.3.2 The Presence of Compressive Reinforcement

In the case of doubly reinforced beam sections, compressive reinforcement is the additional parameter that should be taken into consideration. Its presence increases the ductility of the members with a very small change in yield moment [9].

III. Yielding Point:

To simplify the process, the stress-strain relationship is assumed to be linear.

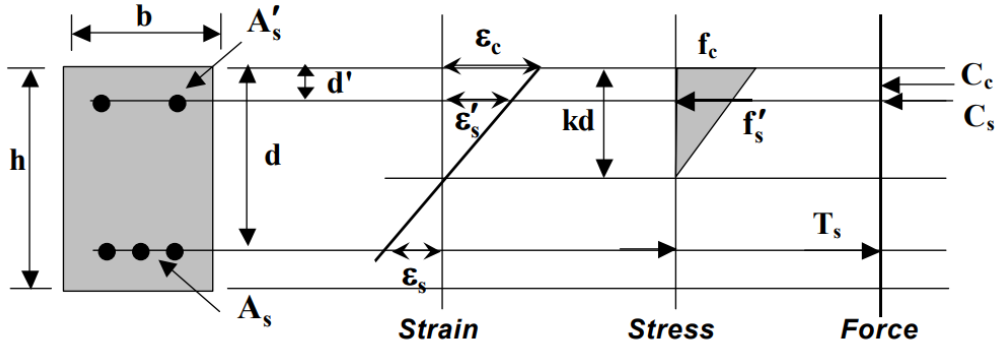


Figure 35. Stress Block at yielding point of doubly reinforced beam [9]

$$\sum F_x = 0$$

$$T_s = C_c + C_s$$

$$A_s * f_s = \frac{1}{2} * f'_c * b * k * d + A_s * f'_s$$

Steel stresses are calculated from the strain compatibility:

$$\frac{\epsilon_c}{k * d} = \frac{\epsilon'_s}{k * d - d'} = \frac{\epsilon_s}{d - k * d}$$

$$f'_s = \frac{k * d - d'}{k * d} * n * f'_c \quad \text{and} \quad f_s = \frac{1 - k}{k} * n * f'_c$$

Substituting the above equations:

$$\left(\frac{1 - k}{k}\right) * A_s * n * f'_c = \frac{1}{2} * f'_c * b * k * d + \left(\frac{k * d - d'}{k * d}\right) * A_s * n * f'_c$$

$$k = \sqrt{(\rho + \rho')^2 * n^2 + 2 * \left(\rho + \rho' * \frac{d'}{d}\right) * n - (\rho - \rho') * n} \quad (\text{Equation 71})$$

Where:

$$\rho = \frac{A_s}{b * d} \quad (\text{Equation 72})$$

$$\rho' = \frac{A'_s}{b * d} * n * f'_c \quad (\text{Equation 73})$$

Finally, the yield moment and curvature at the yield point are:

$$M_y = A_s * f_y * jd \quad (\text{Equation 74})$$

$$\phi_y = \frac{f_y}{d * E_s * (1 - k)} \quad (\text{Equation 75})$$

Where jd is the distance from the tensile reinforcement to the centroid of the compression force.

$$jd = d - \frac{C_c * \frac{k*d}{3} + C_s * d'}{C_c + C_s} \quad (\text{Equation 76})$$

IV. Ultimate Load:

At this point, the compression reinforcement is yielding.

$$k = \frac{f_y * (A_s - A'_s)}{\alpha * f'_c * b * d} \quad (\text{Equation 77})$$

And the ultimate moment and curvature at this point are:

$$M_u = \alpha * f'_c * b * k * d^2 * (1 - k * \gamma) + A'_s * f_y * (d - d') \quad (\text{Equation 78})$$

$$\phi_u = \frac{0,004}{k * d} \quad (\text{Equation 79})$$

3.3.3 Comparison with worked examples

Let's consider the following cross-section and calculate the moment-curvature according to the Kent-Park model when compressive reinforcement is absent and present.

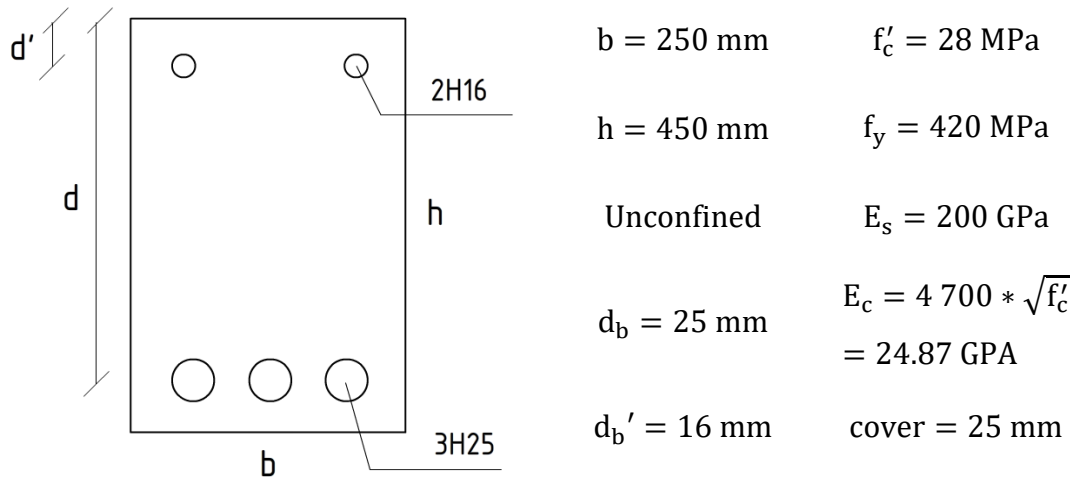


Figure 36. Example of an unconfined concrete section

The moment and curvature values for each critical point are calculated and demonstrated in *Table 4*:

Table 4. Calculated Moment-Curvature values

Compressive RC	Not present		Present	
	Moment (kN m)	Curvature (1/m)	Moment (kN m)	Curvature (1/m)
0	0.00	0.000000	0.00	0.000000
Before Cracking	39.73	0.000713	32.56	0.000713
Cracking	39.73	0.000713	32.56	0.000668
Yield	219.61	0.008434	220.32	0.006000
Ultimate	205.01	0.031003	219.28	0.036500

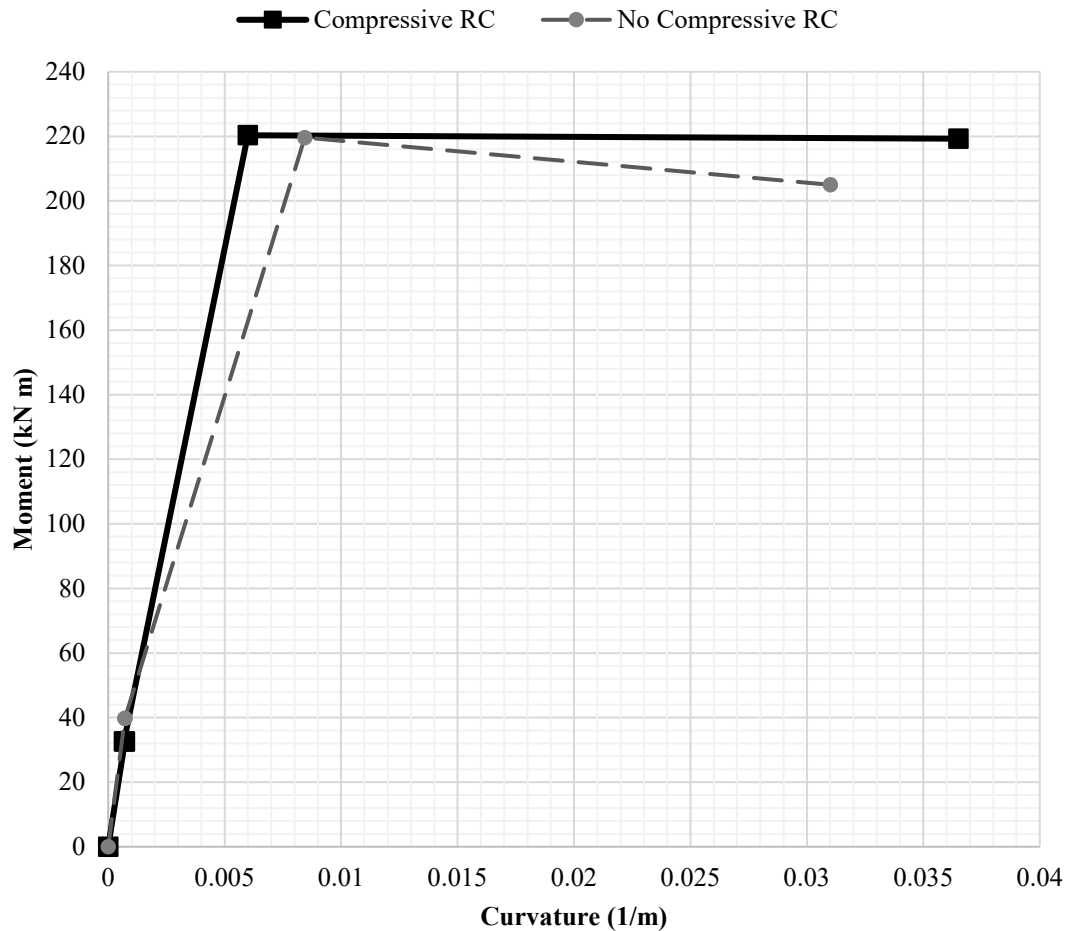


Figure 37. Graphic representation of the moment-curvature data

The shape of the moment-curvature curve can be observed from *Figure 37*. The presence of compressive longitudinal reinforcement increases the moment capacity slightly compared to the case without compressive reinforcement, as stated earlier.

3.3.4 The Presence of Transverse Reinforcement

To improve the ductility and shear performance of the member the longitudinal reinforcement is confined with transverse reinforcement, such as steel stirrups. A confinement zone will be formed in the cross-section.

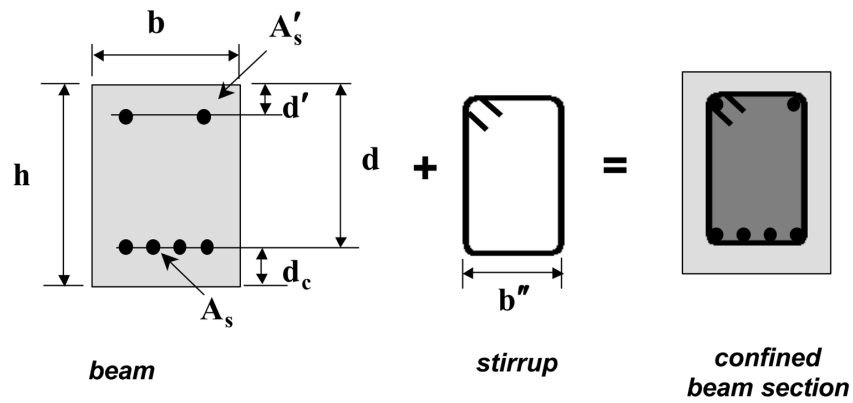


Figure 38. Confined Beam Section [9]

The procedure for determining the moment-curvature relationship of confined concrete sections is the same as the one explained in the previous chapters. The Modified Kent-Park model is adopted due to the presence of confinement, where the confinement factors are introduced [28].

3.4 Moment-Rotation Relationship

Plastic hinges are lumped masses where the concentration of the plastic deformation is accumulated due to bending. These regions are formed when steel reaches its yield point, and their location is determined by the moment-curvature relationship of the cross-section. The moment-rotation relationship describes the behaviour of the member due to bending [9].

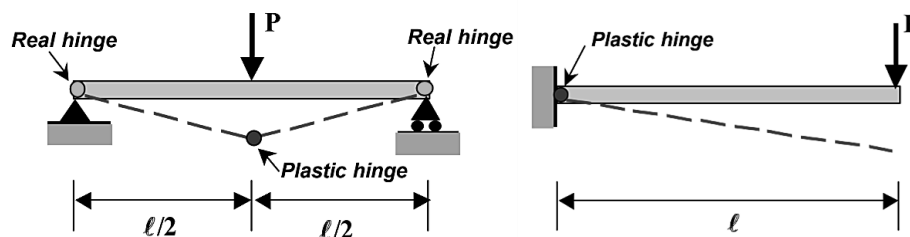


Figure 39. Typical location of plastic hinges [9]

The rotation of the member is determined by the integration of the curvature along the length of the member, including the elastic and plastic regions.

$$\theta = \phi * \ell_p \quad (\text{Equation 80})$$

Where:

$\theta = \text{rotation angle}$

$\phi = \text{curvature length}$

$\ell_p = \text{plastic hinge length}$

There is still no compromise on the best way to estimate the length of plastic hinges, thus researchers have proposed empirical formulas for different types of reinforced concrete beams and columns. Some of the most common methods for calculating the plastic hinge length are:

Table 5. Empirical equations for calculating the length of plastic hinges [29]

Researcher	Plastic Hinge Length, l_p
Baker (1956)	$k \left(\frac{z}{d}\right)^{\frac{1}{4}} d$
Sawyer (1964)	$0.25d + 0.075z$
Corley (1966)	$0.5d + 0.2\sqrt{d} \left(\frac{z}{d}\right)$
Mattock (1967)	$0.5d + 0.05z$
Priestley and Park (1987)	$0.08z + 6d_b$
Paulay and Priestley (1992)	$0.08z + 0.022d_b f_y$
Sheikh and Khoury (1993)	$1.0h$
Coleman and Spacone (2001)	$\frac{G_f^c}{\left[0.6f_c' \left(\varepsilon_{20} - \varepsilon_c + \frac{0.8f_c'}{E_c}\right)\right]}$
Panagiotakos and Fardis (2001)	$0.18z + 0.02ld_b f_y$

Bae and Bayrak (2008)

$$\frac{l_p}{h} = \left[0.3 \left(\frac{p}{p_0} \right) + 3 \left(\frac{A_s}{A_g} \right) - 1 \right] \left(\frac{z}{h} \right) + 0.25$$

$$\geq 0.25$$

Where:

A_g = gross area of concrete section

A_s = area of tension reinforcement

d = effective depth

d_b = diameter of longitudinal reinforcement

E_c = Elastic Modulus of concrete

f_c = compressive strength of concrete

f_y = yielding stress of rebars

G_f^c = concrete fracture energy in compression

h = overall depth of section

p = applied axial force

$$p_0 = 0.85 f'_c (A_g - A_s) + f_y A_s \quad (\text{Equation 81})$$

p_0 = nominal axial load capacity per ACI 318 – 05 (2005) [27]

z = shear span

ε_c = peak compressive strain

z is the distance from the critical point to the point of contraflexure. The point of contraflexure is the point where the moment changes sign, and therefore the moment

is zero. In simple terms, z is the length of the member segment from the critical point to the point where the moment is zero.

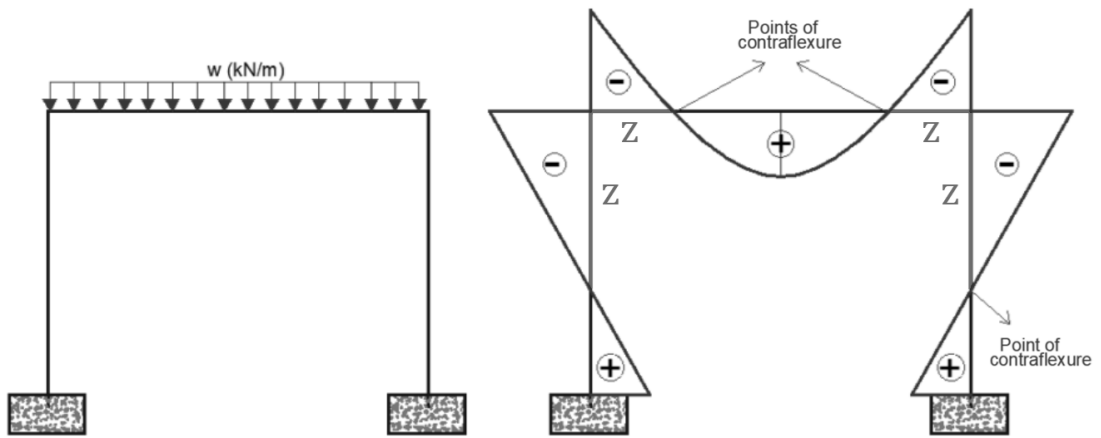


Figure 40. Length of shear spans formed in a frame [30]

CHAPTER 4

CASE STUDY

4.1 Four-Storey Residential Building

The first case study involves the non-linear analysis of a 3D frame of a four-storey residential building located in a seismic zone. It has four bays in both directions with a width of 4 m in the x-direction and 3 m in the y-direction. The frame is modelled using the three concrete models to compare their performance under earthquake loading. The layout of the frame is based on pre-modern building design. The nominal concrete strength is 16 MPa and the steel reinforcement grade is 220 MPa. However, due to the age and quality of construction, the actual concrete strength and stirrup spacing vary throughout the structure. Therefore, two scenarios are considered: one with 16 MPa concrete and 100 mm stirrup spacing, and another with 10 MPa concrete and 250 mm stirrup spacing. These values are obtained from the site surveys conducted on such buildings. The additional information is shown in the following table [31].

Table 6. Data for the first case

	Case 1.1	Case 1.2
Type	Residential Building	
Number of floors	4	
Floor height (m)	2.80	
Bay width in x-direction (m)	4	
Bay width in y-direction (m)	3	
Frame weight (kN)	6830.04	
Concrete cover (mm)	25.00	
Concrete grade (MPa)	16	10
Steel grade (MPa)	220	
Stirrup spacing (mm)	100	250

The longitudinal reinforcement is:

- $8\phi 12$ for the 200x500 beams
- $6\phi 14$ for the 300x300 side columns

- 10 ϕ 14 for the 250x500 / 500x250 columns

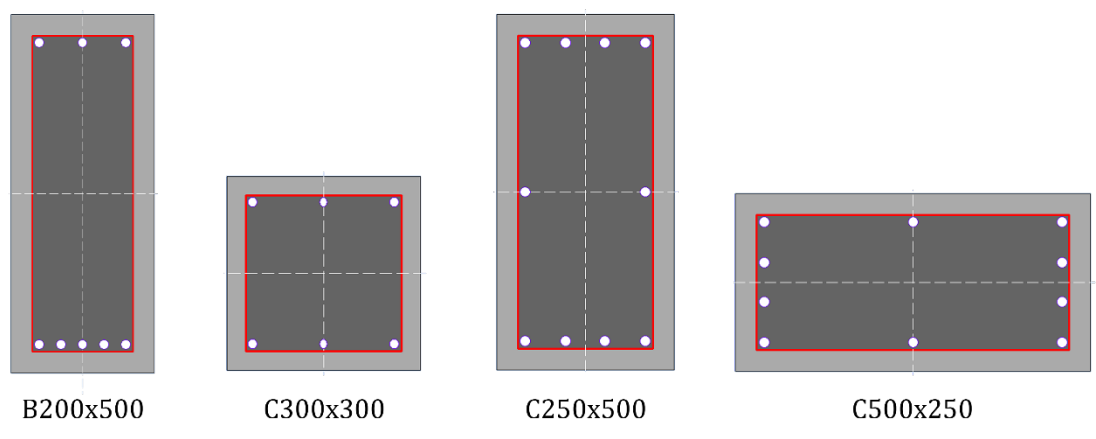


Figure 41. Member cross-sections for the four-storey frame [6]

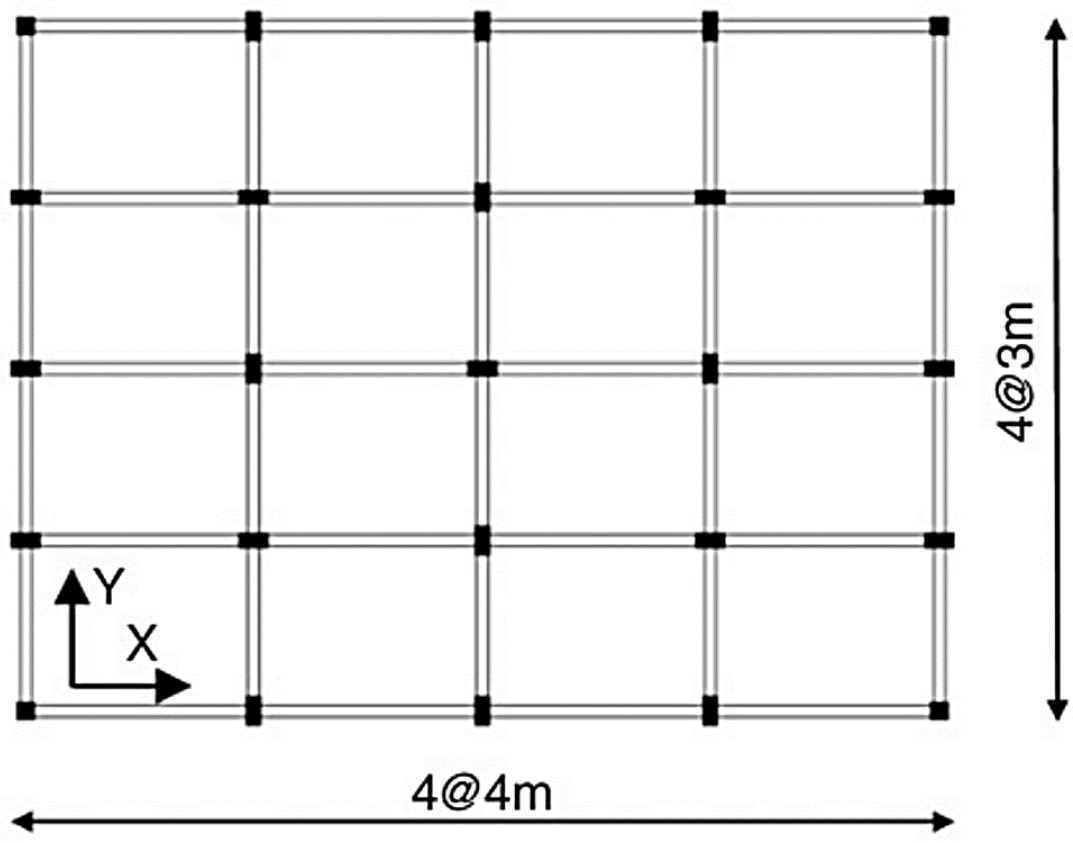


Figure 42. Top view of the frame in xy plan [31]

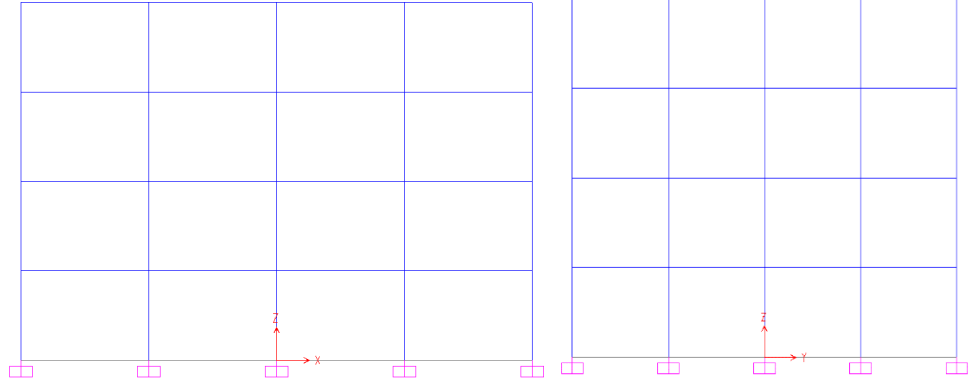


Figure 43. Side views of the frame in xz and yz plans respectively

To evaluate the non-linear behaviour of the structural members, the moment-curvature relationship of each member is calculated using the SEMAp section analysis tool, used by the Scientific and Technical Research Council of Turkey (TÜBİTAK) under Project No. 105M024 [6]. The section is manually configured by inserting the dimensions and reinforcement data.

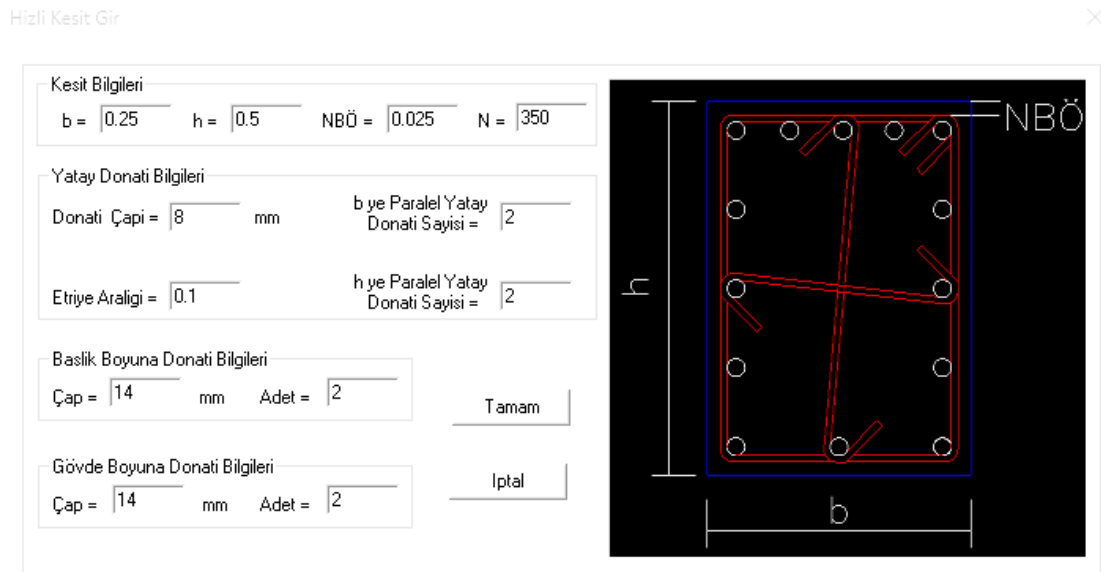


Figure 44. Configuring the section in SEMAp [6]

The initial data for the structural analysis of the building is obtained by running SAP2000 linear analysis with only the dead and live loads ($DL + 0.3LL$) applied to the model. The results show that the average shear span of the beams in the xz-direction is 0.85 m, and the beams in the yz-direction have an average shear span of

0.70 m. The columns have different shear spans for each floor, 1.91 m for the ground floor, 1.44 m for the first and second floors, and 1.50 m for the third floor.

For this study, two representative members are selected for detailed analysis: one of the middle beams in the xz plane (both are symmetric) on the second floor, and the middle column in the xy plane on the ground floor, both belonging to the middle frame of the building. These members have been chosen because they are the most critical in terms of their demand and their influence on the global response of the structure.

The SEMAp section analysis tool is used to calculate the moment-curvature relationship for each concrete model, based on the non-linear material models and the stress-strain relationships of the concrete.

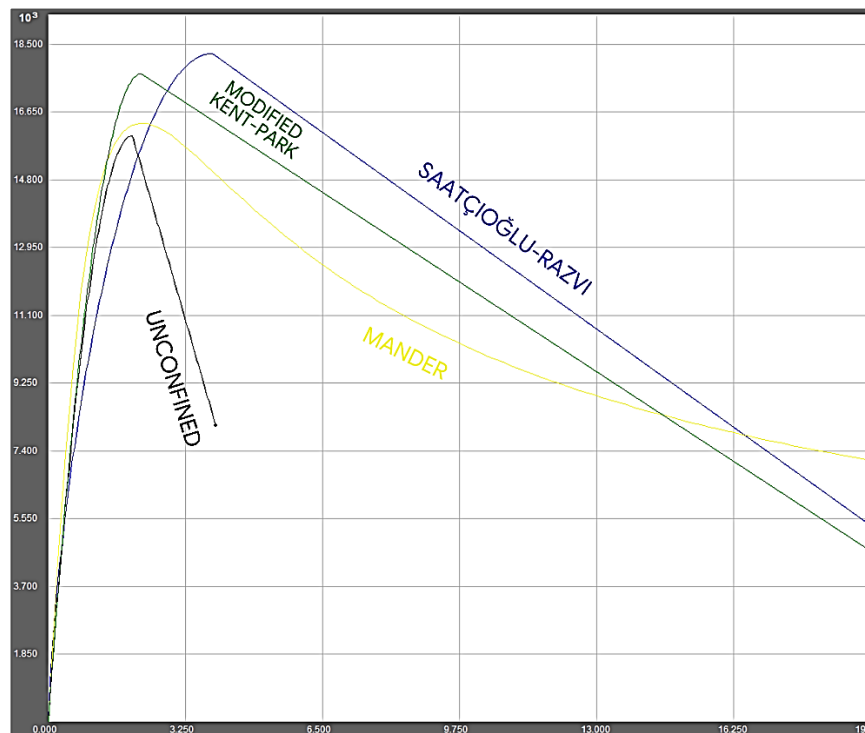


Figure 45. Generated stress-strain curves for the C250x500 column in Case 1.1

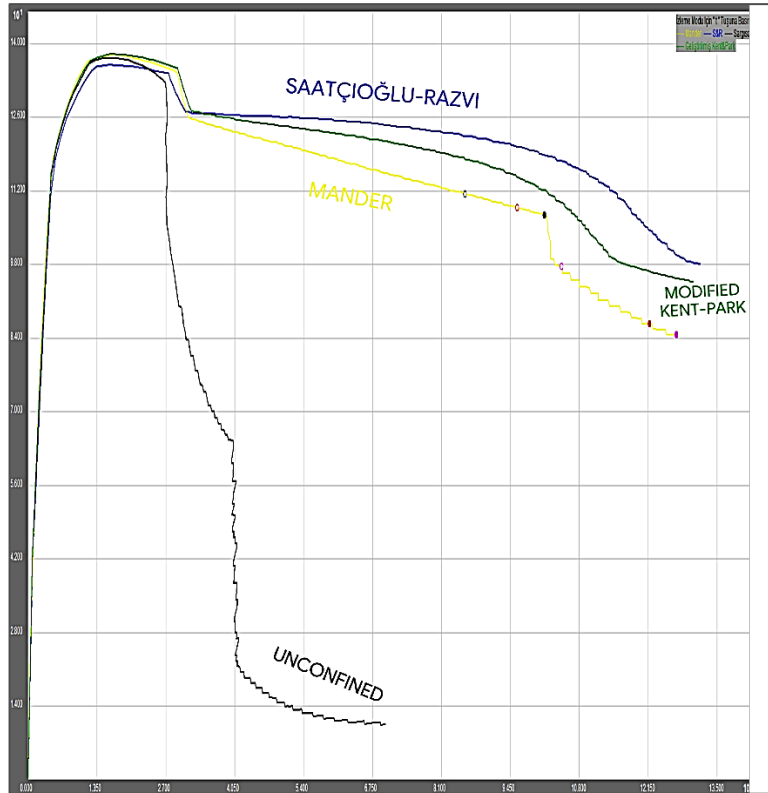


Figure 46. Generated moment-curvature curves for the C250x500 column in Case 1.1

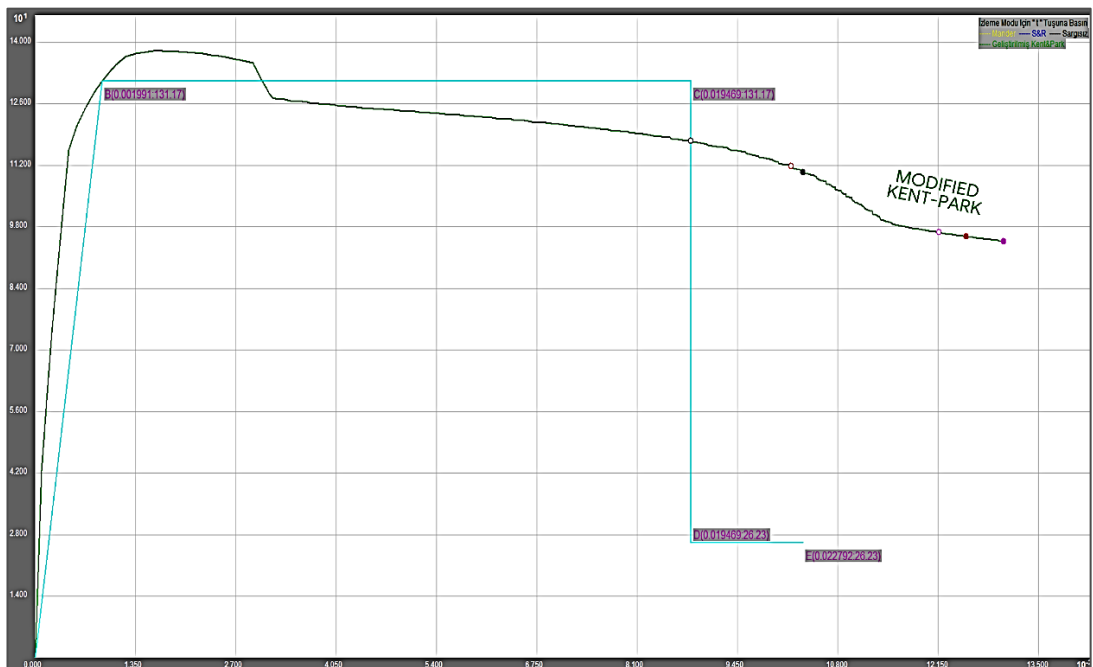


Figure 47. Generated moment-rotation curve for the Modified Kent-Park model of the C250x500 column in Case 1.1

The main difference between the beam and column members in this analysis is the axial force applied to the cross-section. The beam is assumed to have zero axial force, while the column has an axial force of 358 kN, which corresponds to the gravity load on the ground floor. The axial force affects the curvature and the ultimate moment capacity of the member.

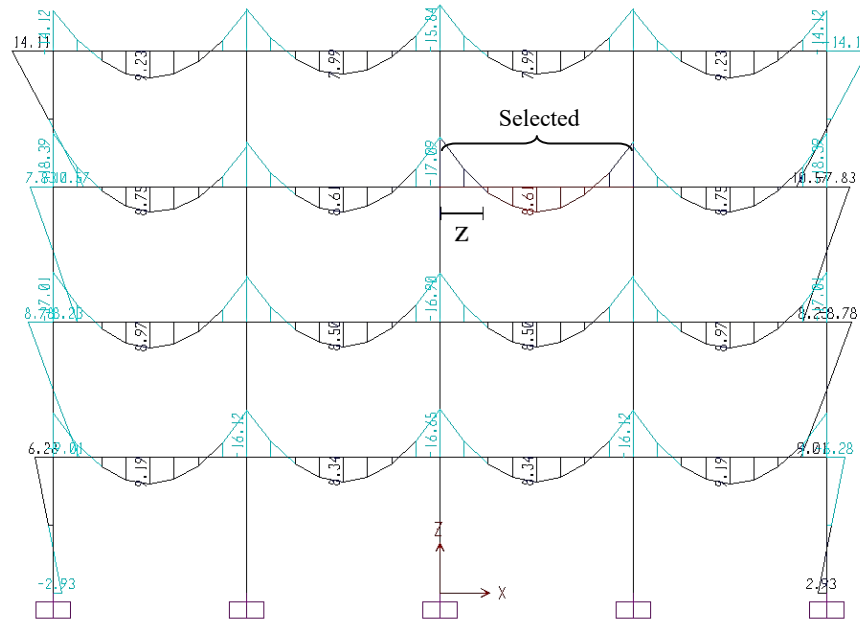


Figure 48. One of the most critical beams in the 4-storey frame

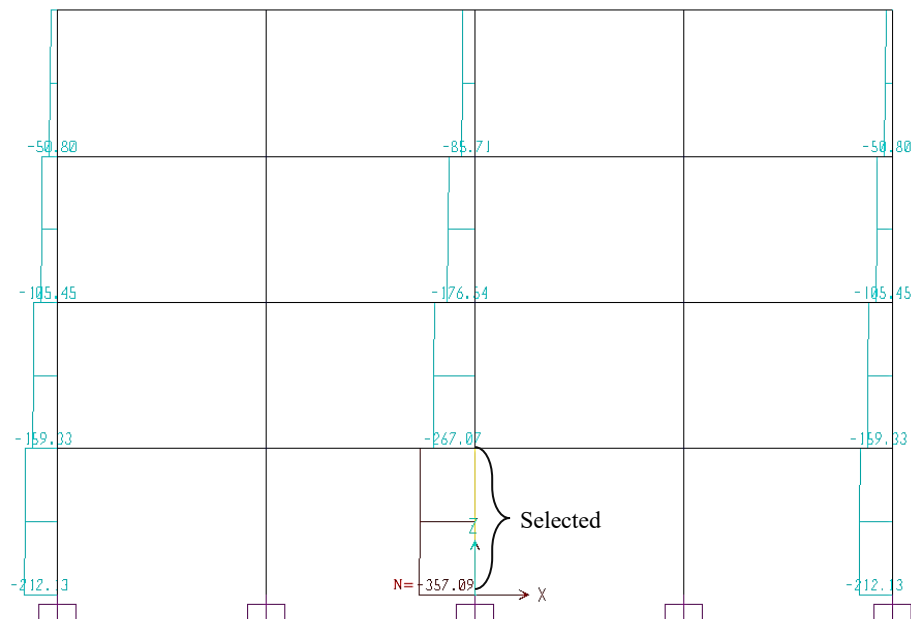


Figure 49. The most critical column in the middle of the frame

The moment-rotation relationship of all members is obtained from the moment-curvature relationship using *Equation 80*. The plastic hinge length is also calculated for each member using Paulay and Priestley's equation from *Table 5*.

The force-deformation and moment-rotation data that is generated for each member is manually assigned to the hinges of the corresponding member in SAP2000. The beams have two degrees of freedom: shear (V2) and moment (M3). The columns have five degrees of freedom: axial (P), shear (V2 and V3), and moment (M2 and M3). The suffixes 1, 2 and 3 denote the local axis of the cross-section of the member, which determines the direction and orientation of the forces and moments acting on the member.

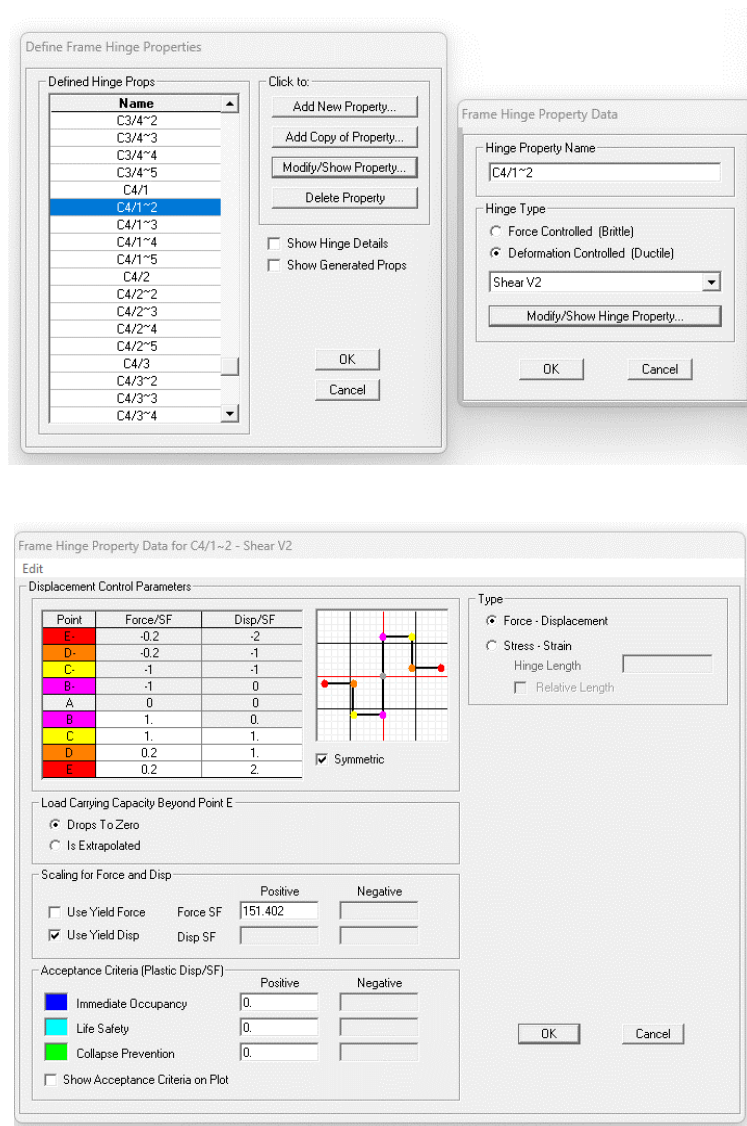


Figure 50. Defining the force-displacement parameters for shear, V2, of column

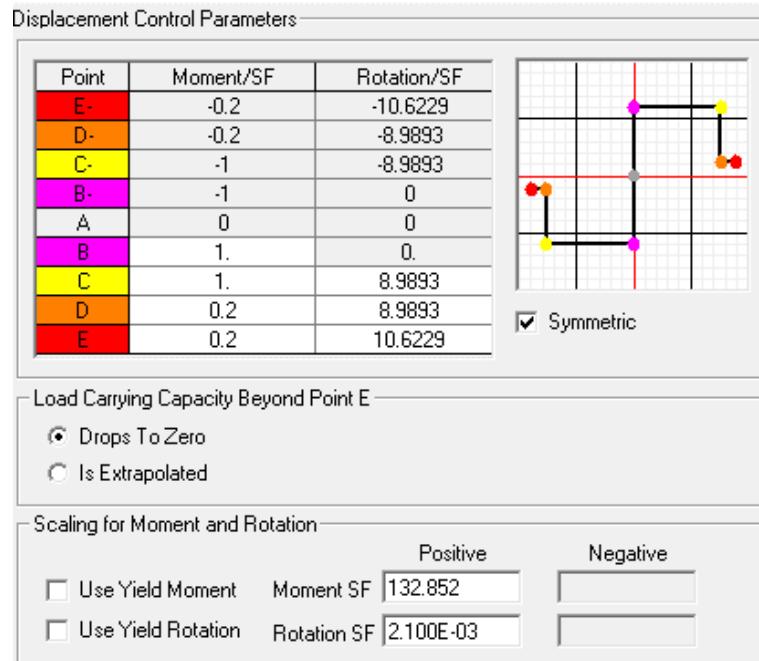


Figure 51. Defining the moment-rotation parameters for moment, M2, of column

The force-displacement and moment-rotation values can be either entered directly into the sheet or divided by safety factors for a clearer presentation.

The next step is performing the non-linear pushover analysis at the global system level, after assigning all the hinges to the frame members. The frame has a natural period of 0.55409 s in the x-direction and 0.54321 s in the y-direction, which reflects its dynamic characteristics and stiffness. The modal load case, which applies a proportional load distribution based on the mode shapes of the frame, is used for conducting the pushover analysis in both directions. The load application control is displacement-controlled, meaning that the load is increased until the target displacement is reached. The target displacement is set to 4% of the frame's height, which is equivalent to 448.0 mm. This value represents the maximum allowable displacement of the frame under seismic loads.

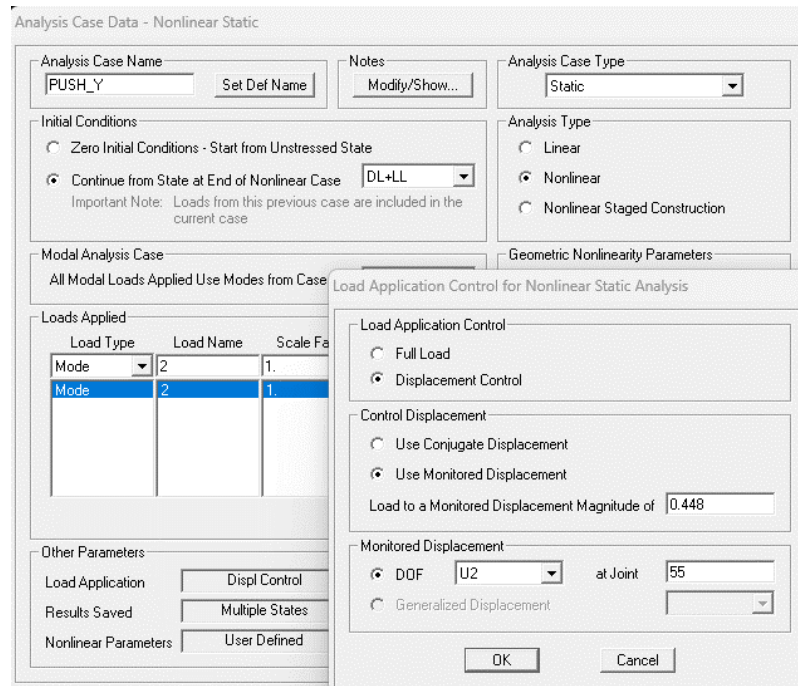


Figure 52. The parameters for the non-linear static pushover analysis in the y-direction

4.2 Seven-Storey Residential Building

The second case study involves the non-linear analysis of a 7-storey frame. The top view of the plan in the xy direction is the same as in *Figure 42*.

Table 7. Data for the second case

	Case 2.1	Case 2.2
Type	Residential Building	
Number of floors	7	
Floor height (m)	2.80	
Bay width in y-direction (m)	4	
Bay width in x-direction (m)	3	
Frame weight (kN)	15,100.96	
Concrete cover (mm)	25.00	
Concrete grade (MPa)	16	10
Steel grade (MPa)	220	
Stirrup spacing (mm)	100	250

The longitudinal reinforcement is:

- $8\phi 14$ for the 250x600 beams
- $12\phi 14$ for the 400x400 side columns
- $8\phi 16$ and $2\phi 14$ for the 300x600 / 600x300 columns

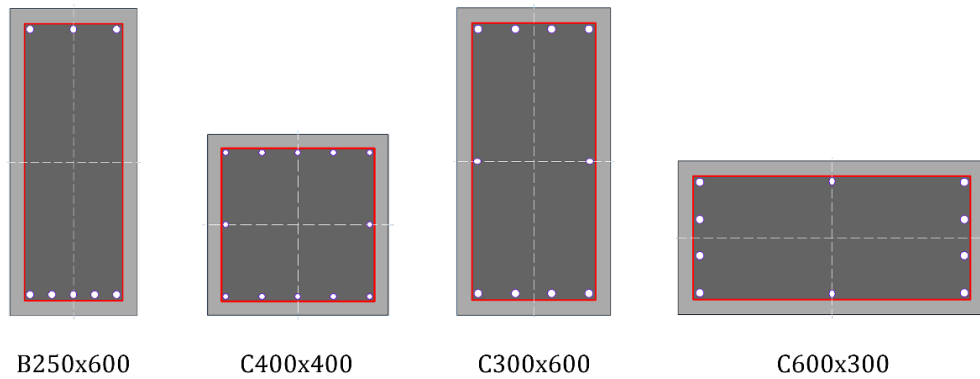


Figure 53. Member cross-sections for the seven-storey frame [6]

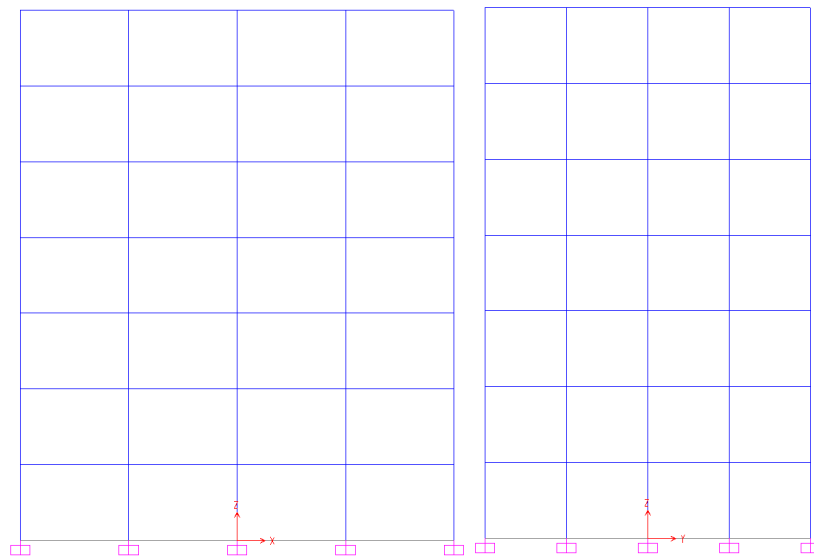


Figure 54. Side view of the frame in xz and yz plans respectively

For this case, two representative members are selected for detailed analysis too: one of the side beams in the xz plane (both are symmetric) on the sixth floor, and the middle column in the xy plane on the ground floor, both belonging to the middle frame of the building.

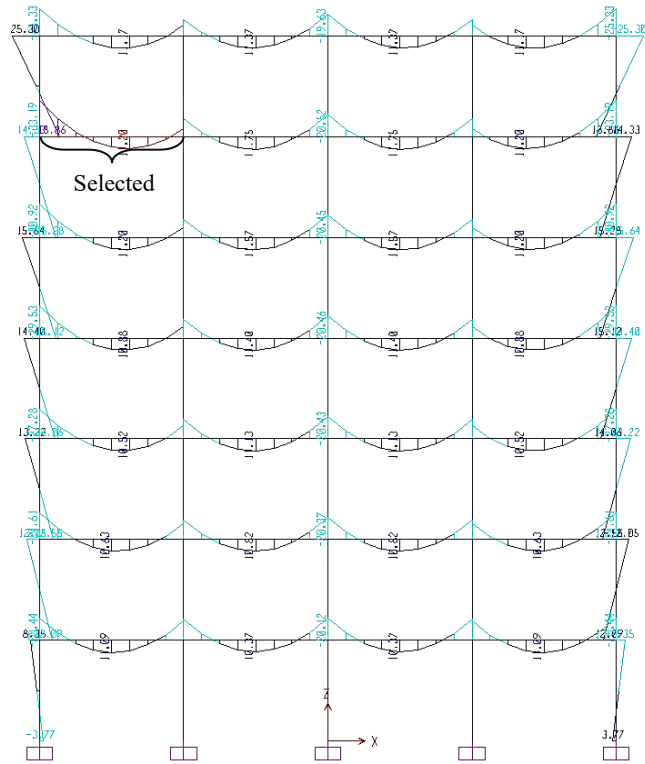


Figure 55. One of the most critical beams in the 4-storey frame

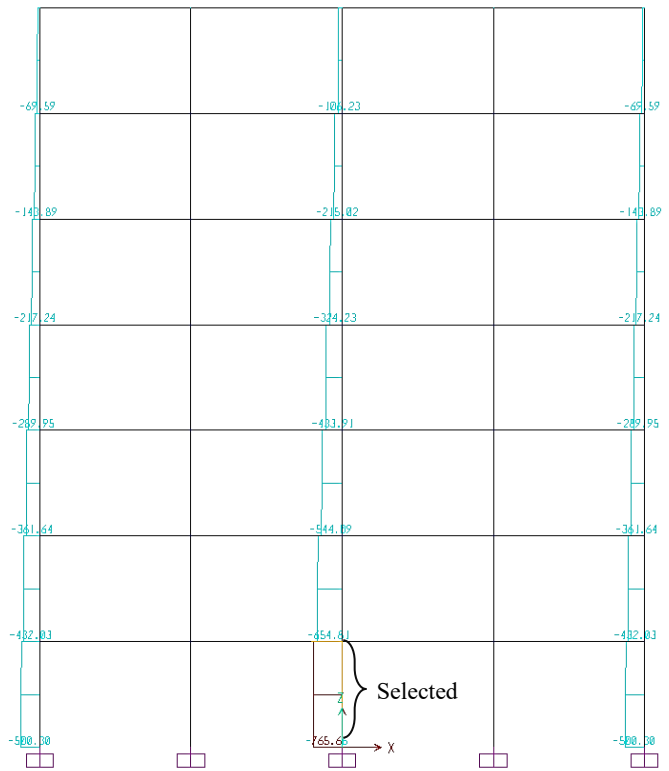


Figure 56. The most critical column in the middle of the frame

The frame has a natural period of 0.76456 s in the x-direction and 0.75352 s in the y-direction. The target displacement is set to 4% of the frame's height, which is equivalent to 784.0 mm.

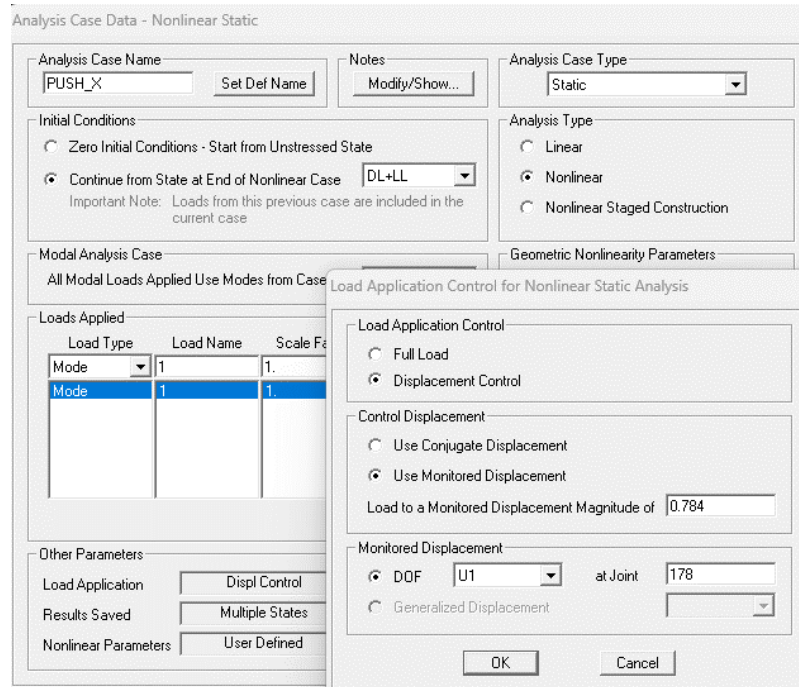


Figure 57. The parameters for the non-linear static pushover analysis in the x-direction

CHAPTER 5

RESULTS AND DISCUSSIONS

5.1 Results

A comparison of the moment-curvature relationships of the beam and column sections for different concrete models reveals that the concrete behaviour in the column case is more sensitive to the choice of the model than in the beam case. This happens due to the presence of axial loads and confinement effects of the column, which affect the concrete behaviour and strength. The axial load reduces the curvature and increases the ultimate moment capacity of the column, while the confinement effect enhances the concrete strength and ductility by preventing lateral expansion and cracking.

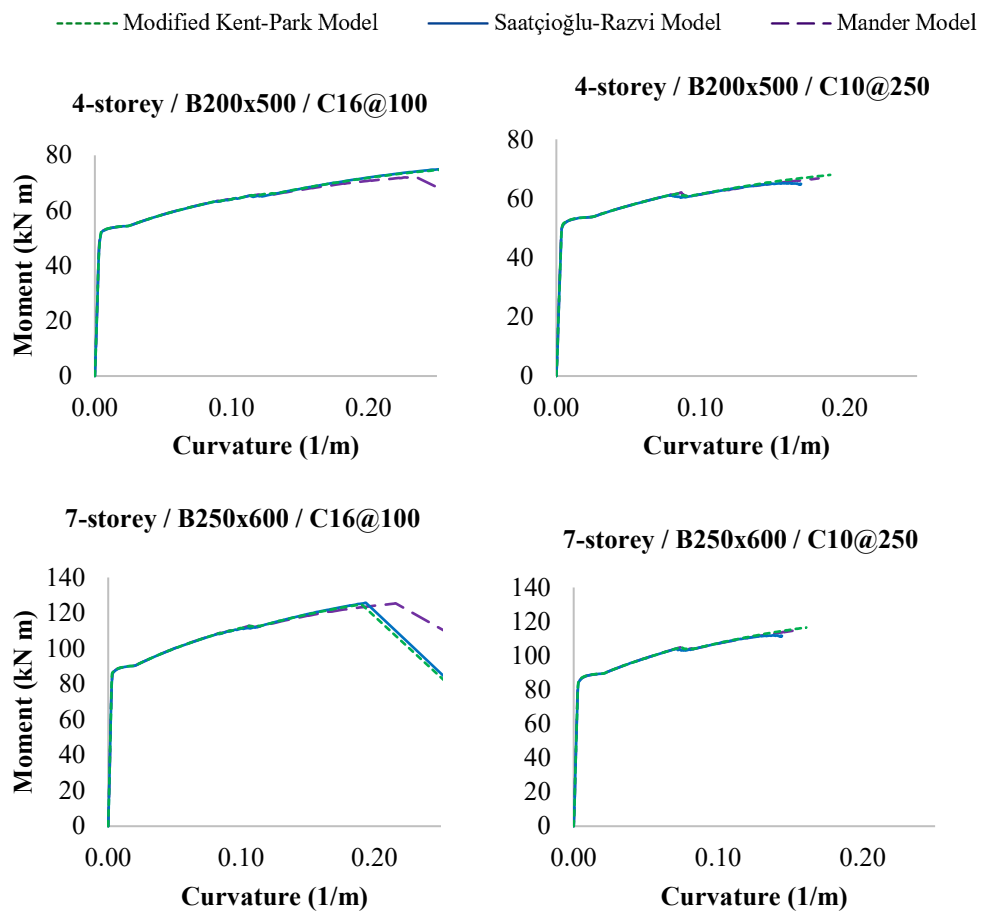


Figure 58. Moment-curvature data for the selected beam sections

- - - Modified Kent-Park Model
 — Saatçioğlu-Razvi Model
 - - - Mander Model

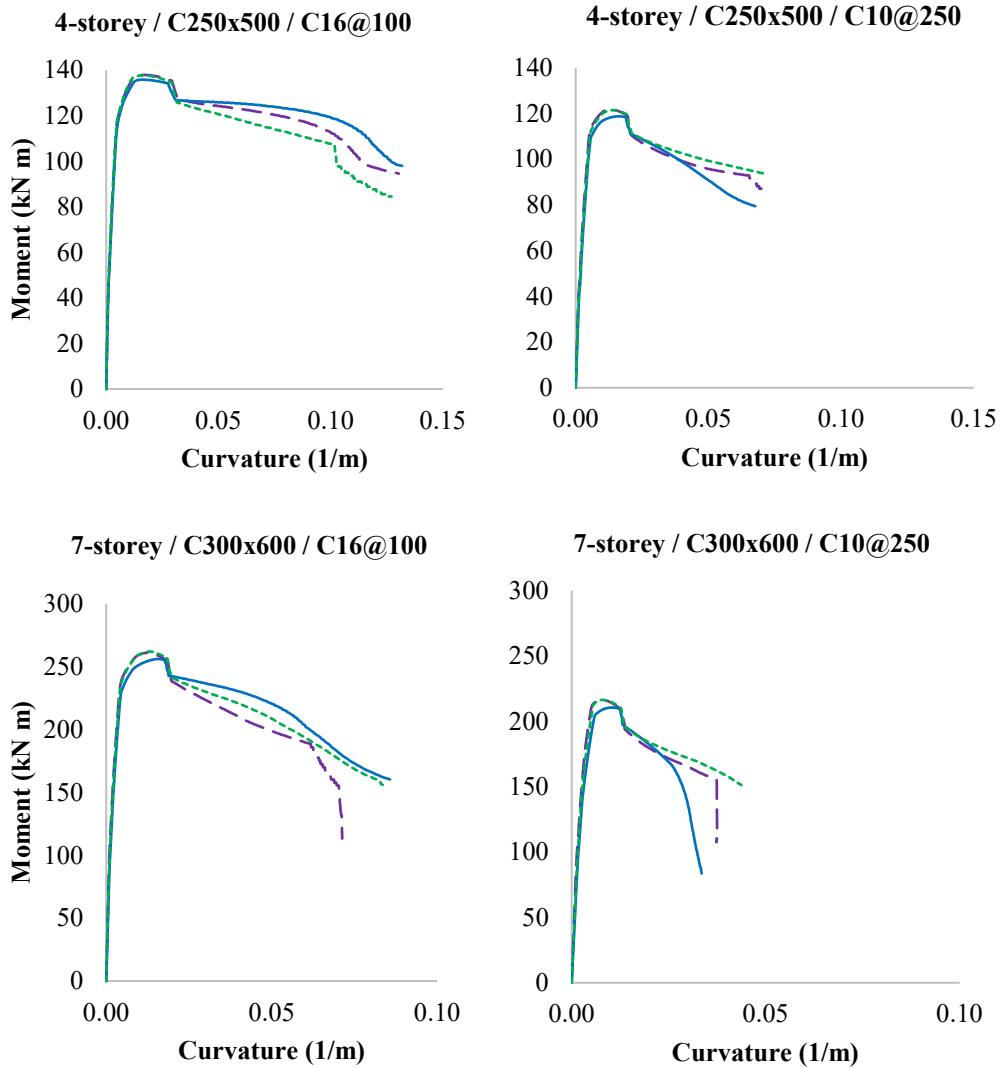


Figure 59. Moment-curvature data for the selected column sections

Another factor that influences the moment-curvature of the members is the stirrup spacing and concrete quality. As expected, the members with smaller stirrup spacing and better concrete quality have higher moment capacity than the members with larger stirrup spacing and poor concrete quality. This is because the stirrups provide confinement and shear resistance to the concrete, while the concrete quality affects the compressive strength and stiffness of the material. Moreover, the strain capacity of the members, which represents their ductility and deformation ability, is lower when the concrete quality is poor and the stirrup spacing is large, especially in

the seven-story case. This indicates that these members are more prone to brittle failure and less able to dissipate energy under seismic loads.

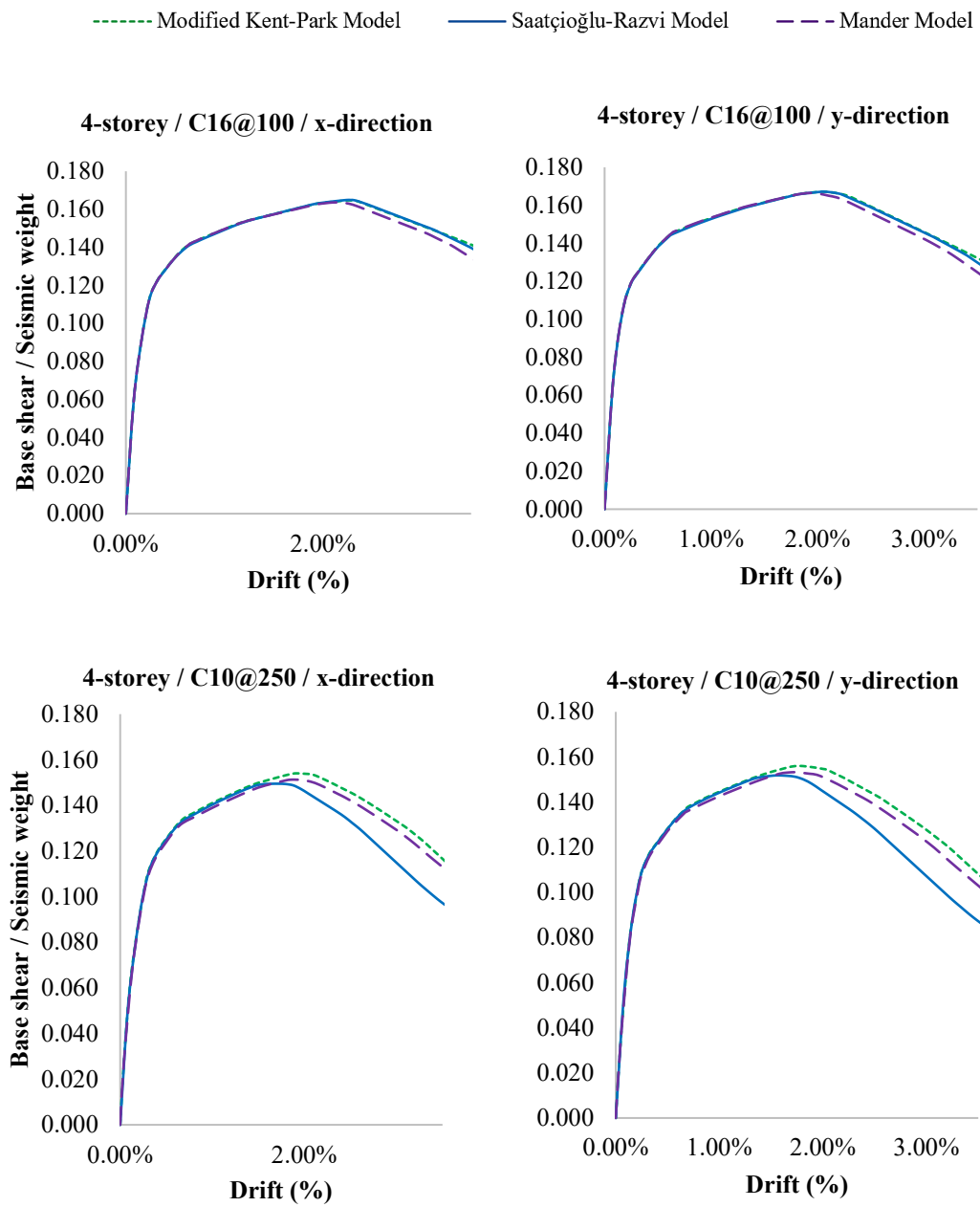


Figure 60. Capacity curves for the four-storey frame

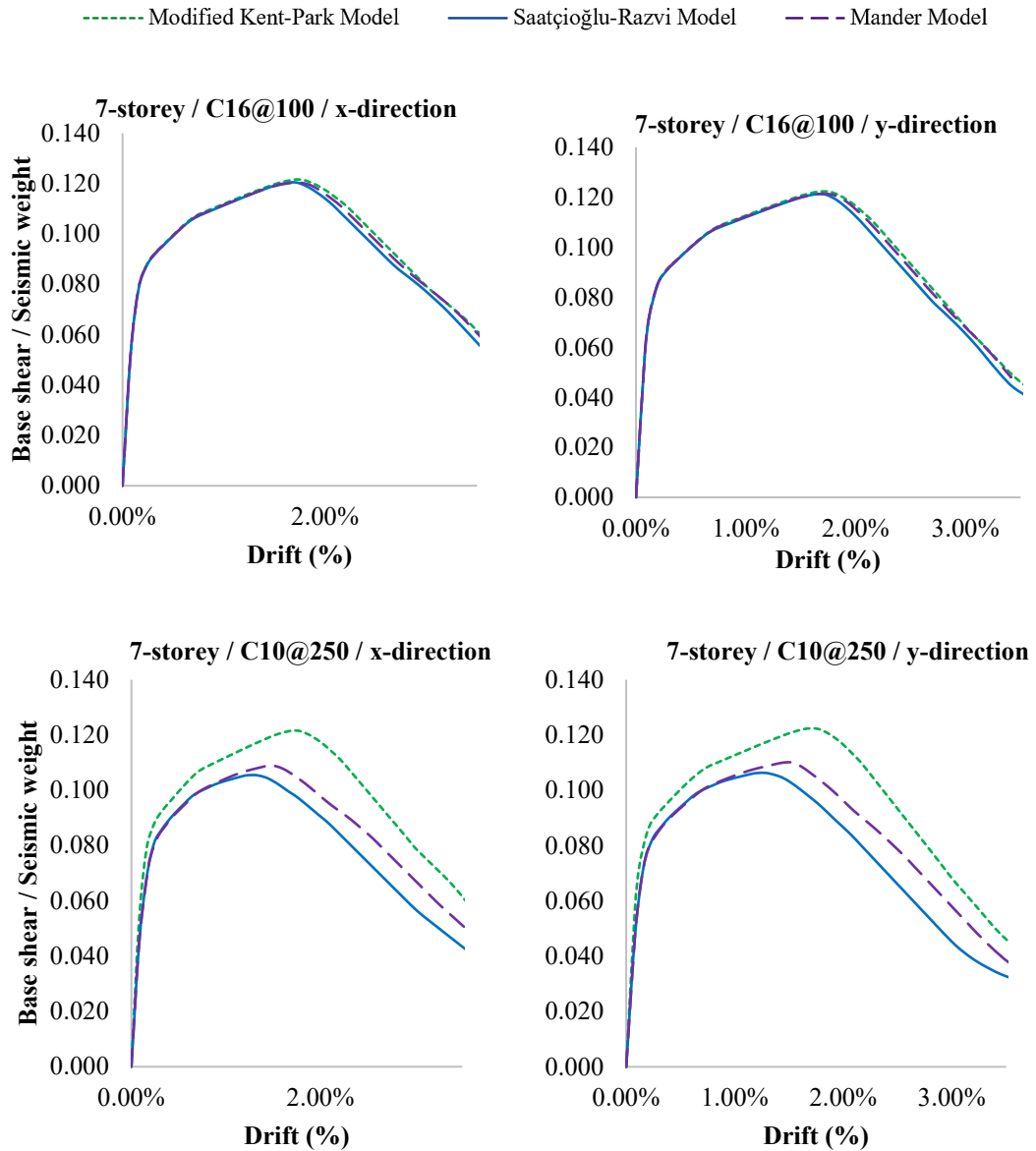


Figure 61. Capacity curves for seven-storey frame

The final observation is made on the capacity curve of the frames, which is obtained from the non-linear pushover analysis. The capacity curve shows the base shear versus the roof displacement of the frame under lateral loads. The results show that the capacity curve is not sensitive to the choice of the concrete model, as all the models produce similar curves for both frames. However, the capacity curve is influenced by the concrete grade and the stirrup spacing of the members, as these factors affect the moment capacity and ductility of them. The frames with better concrete grade and smaller stirrup spacing have a higher base shear and roof displacement than the frames with poor concrete grade and larger stirrup spacing. This

means that these frames have higher strength and deformation capacity. The effect of the concrete grade and stirrup spacing is more evident in the seven-story frame than in the four-story frame, as the seven-story frame has more members and more gravity load than the four-story frame. Therefore, these factors are important for designing and evaluating the seismic performance of reinforced concrete frames.

CHAPTER 6

CONCLUSIONS

6.1 Conclusions

The main objective of this thesis was to compare the different concrete models in SAP2000 for the non-linear analysis of reinforced concrete frames under seismic loads. The concrete models were applied to the cross-sections of the beam and column members of two frames: a four-story frame and a seven-story frame. The moment-curvature and moment-rotation relationships of the members were calculated using the SEMAp section analysis tool, which was developed by the Scientific and Technical Research Council of Turkey (TÜBİTAK) under Project No. 105M024. The force-deformation and moment-rotation data were then manually assigned to the hinges of the corresponding members in SAP2000. The non-linear pushover analysis was performed on the frames using the modal load case and the displacement-controlled load application.

The results show that the concrete models have a significant effect on the moment-curvature and moment-rotation relationships of the members, especially in the column case. The concrete models also affected the plastic hinge length and the strain capacity of the members, which are important parameters for evaluating the ductility and energy dissipation of the structure. However, the concrete models did not have a noticeable effect on the capacity curve of the frames, which showed similar base shear / seismic weight and drift values for all models. The capacity curve is more influenced by the concrete grade and the stirrup spacing of the members, which affected the strength and deformation capacity of the frames. The effect of these factors is more pronounced in the seven-story frame than in the four-story frame, due to the higher number of members and gravity load. Therefore, it can be concluded that the selection of an appropriate concrete model for the non-linear analysis of reinforced concrete frames is crucial for capturing the local behaviour and performance of the members, while the selection of an appropriate concrete grade and stirrup spacing is crucial for capturing the global behaviour and performance of the frames.

6.2 Recommendations for future research

As stated before, this thesis compared the different concrete models at local and global system levels. However, there are still some limitations and challenges that need to be addressed in future research. For example, more concrete models can be investigated and validated using experimental data and other software tools. More frames with different geometries, heights, and boundary conditions can be analysed and compared using the same concrete models. More concrete grades and stirrup spacings can be considered and their effects on the moment-curvature, moment-rotation, and capacity curve of the frames can be evaluated. These aspects can provide more insights and understanding of the non-linear behaviour and performance of reinforced concrete frames under seismic loads and can help to improve the design and assessment of these structures.

REFERENCES

- [1] V. Perumal, K. S and A. K. B, “Comparative Study of Stress-Strain Confined Concrete Models,” *International Journal of Scientific & Engineering Research*, vol. 11, no. 12, pp. 926-932, 2020.
- [2] A. S. Elnashai and L. D. Sarno, *Fundamentals of Earthquake Engineering*, 1st ed., Wiley, 2008, p. 347.
- [3] D. C. Kent and R. Park, “Flexural Members with Confined Concrete,” *Journal of the Structural Division*, vol. 97, no. 7, pp. 1969-1990, 1971.
- [4] M. Y. KALTAKCI, A. KÖKEN and Ü. S. YIMAZ, “Experimentally and Analytical Investigation of Axially Loaded Tied Columns with and without Steel Fibers,” *Dokuz Eylul University Journal*, vol. 8, no. 1, pp. 65-85, 2006.
- [5] J. B. Mander, M. J. N. Priestley and R. Park, “Theoretical Stress-Strain Model for Confined Concrete,” *Journal of Structural Engineering*, vol. 114, no. 8, pp. 1804-1826, 1988.
- [6] M. Inel, H. B. Özmen and H. Bilgin, “Computer Modeling of Translinear Behaviors of Reinforced Concrete Elements (SEMAp),” *The Scientific and Technological Research Council of Turkey (TÜBİTAK)*, 2008.
- [7] Computers and Structures, Inc., “SAP2000 Non-linear Structural Software,” Berkeley, California, USA, 2007.
- [8] Committee E-701, *Reinforcement for Concrete - Materials and Applications*, ACI Education Bulletin E2-00, 2006, p. 16.
- [9] M. Sözen, *Stiffness of RC Members / CE 676 Behavior of Reinforced Concrete Members*, Purdue University, 2001.
- [10] F. U. Rahman, “What is Rebar? Types and Grades of Steel Reinforcement,” *The Construction Encyclopedia*.

- [11] Anping County Wennian Wire Mesh Products Co., Ltd., “Rebar Sizes of Different Standards,” [Online]. Available: <https://www.reinforcing-bar.com/technology/reinforcing-bar-sizes.html>.
- [12] O. Farghal, H. Mohamed and A. Diab, “Prediction of axial compressive strength of reinforced concrete circular short columns confined with carbon fiber reinforced polymer wrapping sheets,” *Journal of Reinforced Plastics and Composites*, vol. 32, no. 19, pp. 1406-1418, 2013.
- [13] P. Jadhav, “Rectangular versus Parabolic Stress Block Design for IRS,” 2022.
- [14] F. U. Rahman, “Tension Test on Steel Rod - Procedure and Results,” The Construction Encyclopedia.
- [15] E. Canbay, G. Ozcebe and U. Ersoy, “High-Strength Concrete Columns under Eccentric Load,” *Journal of Structural Engineering @ ASCE*, vol. 132, no. 7, pp. 1052-1060, 2006.
- [16] CEN, “Eurocode 3: Design of steel structures - Part 1-1: General rules”. 2005.
- [17] ASTM, “Standard Specification for Deformed and Plain Low-Alloy Steel Bars for Concrete Reinforcement”. Patent ASTM A706.
- [18] A. J. Hamad, “Size and shape effect of specimen on the compressive strength of HPLWFC reinforced with glass fibres,” *Journal of King Saud University - Engineering Sciences*, vol. 29, no. 4, pp. 373-380, 2015.
- [19] X. Pang, “Beneficial Use of Spent Mushroom Substrate in the Construction Industry,” Villanova University, 2007.
- [20] A. K. Samani and M. M. Attard, “A stress–strain model for uniaxial and confined concrete under compression,” *Engineering Structures*, vol. 41, pp. 335-349, 2012.

- [21] S. Shen, “A step-by-step anatomy of concrete stress-strain curve,” The Si-Eng, 2021.
- [22] A. Sharma, G. Reddy, K. Vaze, R. Eligehausen and J. Hofmann, “Nonlinear Seismic Analysis of Reinforced Concrete Framed Structures Considering Joint Distortion,” *BARC--2011/E/026*, vol. 43, no. 30, p. 278, 2012.
- [23] S. Popovics, “A numerical approach to the complete stress-strain curve of concrete,” *Cement and Concrete Research*, vol. 3, no. 5, pp. 583-599, 2003.
- [24] S. A. Sheikh and S. Uzumeri, “Analytical Model for Concrete Confinement in Tied Columns,” *Journal of the Structural Division*, vol. 108, no. 12, pp. 2703-2722, 1982.
- [25] D.-C. Feng and Z. Ding, “A new confined concrete model considering the strain gradient effect for RC columns under eccentric loading,” *Magazine of Concrete Research*, vol. 70, no. 23, pp. 1189-1204, 2018.
- [26] V. V. Cao and H. R. Ronagh, “A model for damage analysis of concrete,” *Advances in Concrete Construction*, vol. 1, no. 2, pp. 187-200, 2013.
- [27] American Concrete Institute, *Building Code Requirements for Reinforced Concrete*, Detroit, MI.
- [28] H. Bilgin and B. Plaku, “Influence of confined concrete behavior on RC moment resisting frames,” in *Second International Conference of Civil Engineering (ICCE 2023)*, Tirana, Albania, 2023.
- [29] X. Zhao, Y.-F. Wu, A. Leung and H. F. Lam, “Plastic Hinge Length in Reinforced Concrete Flexural Members,” *Procedia Engineering*, vol. 14, pp. 1266-1274, 2011.
- [30] U. Obinna, “Point of Contraflexure in Structures,” Structville, 2022.

- [31] M. Inel, H. B. Ozmen and H. Bilgin, “Re-evaluation of building damage during recent earthquakes in Turkey,” *Engineering Structures*, vol. 30, no. 2, pp. 412-427, 2008.
- [32] T. Bhujangrao, C. Froustey, E. Iriondo, F. Veiga, P. Darnis and F. G. Mata, “Review of Intermediate Strain Rate Testing Devices,” *Metals - Open Access Metallurgy Journal*, vol. 10, no. 7, pp. 894-918, 2020.